applied sciences

MDPI

Article

Phoenician Pottery in the Western Mediterranean: A New Perspective Based on the Early Iron Age (800–550 BC) Settlement of Sant Jaume (Alcanar, Catalonia)

Eva Miguel Gascón [1,*], Jaume Buxeda i Garrigós [1,2], Peter M. Day [3,4] and David Garcia i Rubert [2,5]

1 Cultura Material i Arqueometria UB (ARQUB, GRACPE), Department d'Història i Arqueologia, Universitat de Barcelona, Montalegre 6, 08001 Barcelona, Spain; jbuxeda@ub.edu
2 Institut d'Arqueologia de la Universitat de Barcelona (IAUB), Montalegre 6, 08001 Barcelona, Spain; dgarciar@ub.edu
3 Institute of Nanoscience and Nanotechnology, NCSR Demokritos, Agia Paraskevi, 153 41 Athens, Greece; p.m.day@sheffield.ac.uk
4 Department of Archaeology, University of Sheffield, Northgate House, West Street, Sheffield S1 4ET, UK
5 Grup de Recerca en Arqueologia Protohistòrica (GRAP), Department d'Història i Arqueologia, Universitat de Barcelona, Montalegre 6, 08001 Barcelona, Spain
* Correspondence: evamigascon@gmail.com; Tel.: +34-652074805

Abstract: One of the most important reception sites for Phoenician pottery imports in the NE Iberian Peninsula is the Early Iron Age (800–550 BC) settlement of Sant Jaume. This site is exceptional in terms of preservation and the large number of complete vessels recovered. Moreover, the ceramic assemblage comprises one of the best collections of the earliest wheel-thrown pottery that is considered evidence of trade from the western Phoenician colonies and their specific interest in exploiting metallurgical resources. In this research, a sample of 58 individuals of wheel-thrown pottery has been analysed by X-ray fluorescence (XRF), X-ray diffraction (XRD), petrography (PE), and scanning electron microscopy attached with an energy dispersive X-ray unit (SEM-EDX). It was possible to identify 29 ceramic groups, some of which correspond to known Phoenician workshops of southern Andalusia and Ibiza, though the origin of most groups remains to be determined. The wide variety of sources identified illuminates the patterns of trade and exchange that the Phoenicians developed during the Early Iron Age and the export of their manufactured products. This information is fundamental to our understanding of the economic system developed by the Western Mediterranean Phoenician colonies that affected and transformed indigenous communities in the Mediterranean region.

Keywords: Mediterranean Iron Age; Phoenician trade; XRF; XRD; petrography; SEM-EDX; pottery; provenance; diversity

Citation: Miguel Gascón, E.; Buxeda i Garrigós, J.; Day, P.M.; Garcia i Rubert, D. Phoenician Pottery in the Western Mediterranean: A New Perspective Based on the Early Iron Age (800–550 BC) Settlement of Sant Jaume (Alcanar, Catalonia). *Appl. Sci.* **2023**, *13*, 3733. https://doi.org/10.3390/app13063733

Academic Editor: Lola Pereira

Received: 16 January 2023
Revised: 10 March 2023
Accepted: 11 March 2023
Published: 15 March 2023

1. Introduction

The Phoenician arrival in the Iberian Peninsula, attracted by the wealth of metal resources [1], has been the subject of intense debate, primarily because written and archaeological sources differ significantly. Although classical sources point to the foundation of Gadir (Cádiz) by the Tyrians in the 12th century BC, there is no archaeological evidence for the first Phoenician contacts with the southern Iberian Peninsula before the 10th century BC [2,3]. Moreover, the Morro de Mezquitilla [4], La Rabanadilla [5], and the evidence from the Cine Cómico in Cádiz [6] cannot be used to date permanent settlements before the end of the 9th century BC or the beginning of the 8th century BC. At that time, the places used as stopovers on long-distance journeys in the Western Mediterranean became proper urban colonies [7,8] (Figure 1a,b). However, around the middle of the 7th century BC, there was a further expansion of these settlements into surrounding areas. The results were larger settlements, such as the well-documented examples in the region of Vélez-Málaga [9].

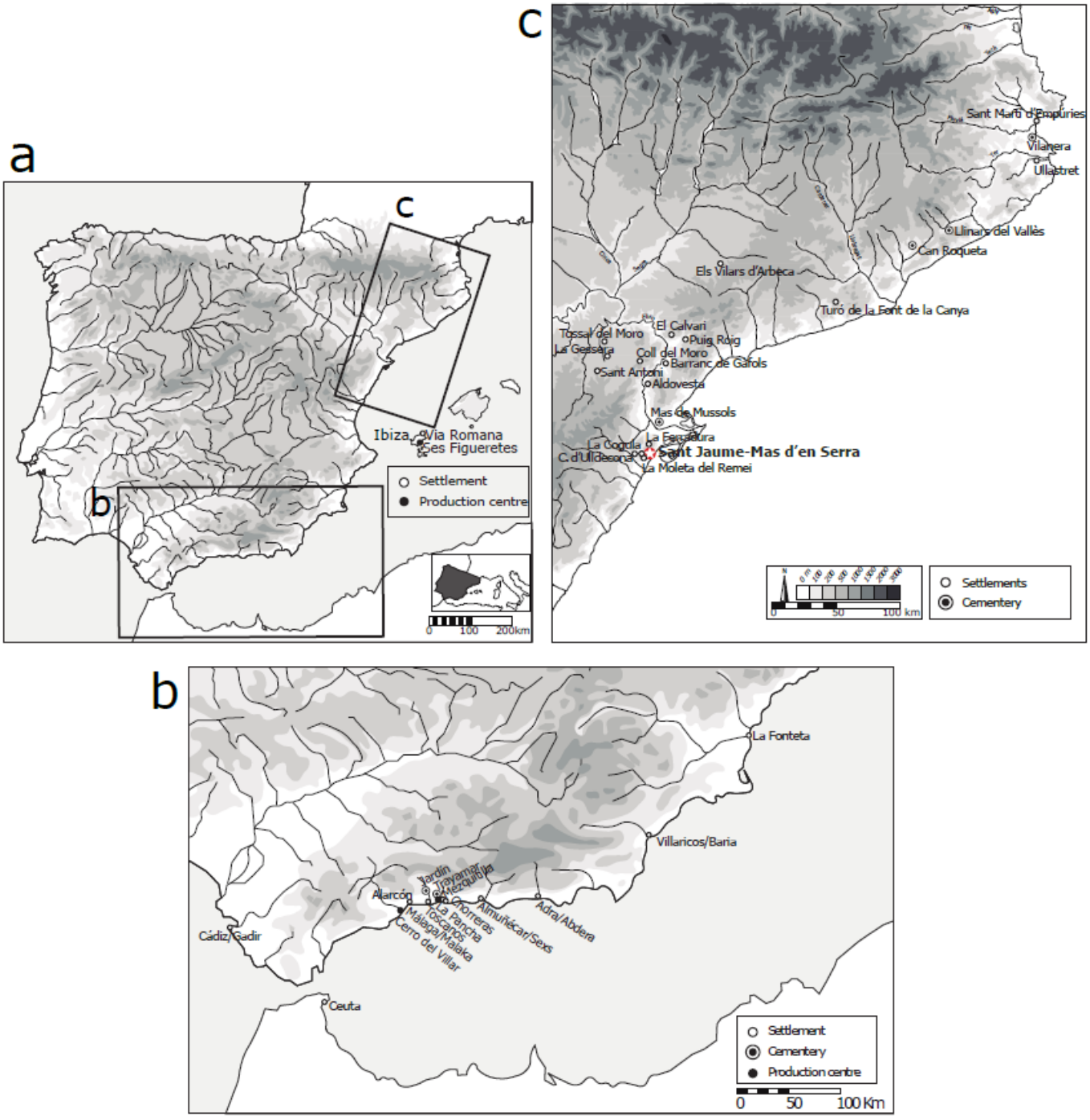

Figure 1. Map of the locations of Phoenician colonies in Ibiza (**a**), on the southeastern coast of the Iberian Peninsula (**b**), and the Early Iron Age reception sites of Phoenician pottery along the northeastern coast (**c**).

The archaeological campaigns undertaken between 1964 and 1984 by the Deutsches Archäologisches Institut (DAI) at the sites of Toscanos, Morro de Mezquitilla, Alarcón, Jardín, Trayamar, and Chorreras [10–15] offered the first ^{14}C dates related to stratigraphic contexts of the beginning of the 8th century BC for some of these early colonies. These excavations also enabled the recovery of large ceramic assemblages of Western Phoenician products, leading to a profound impact on the interpretation of the Early Iron Age archaeological record in the northeastern Iberian Peninsula. Traditionally, the development of the Iberian culture had been discussed in the light of the Greek colonisation, but the recognition

of the intense activities of Phoenicians as pioneer traders acted as a timely counterbalance. In fact, the Phoenician presence in the northeastern Iberian Peninsula (Figure 1c), its associated trade network, and the interaction with indigenous communities did not become a key topic in the study of protohistory until the end of the 1960s [16]. From then on, wheel-thrown pottery, identified by typological and macroscopic observations [17–20], was used as an indicator of interaction with the known Phoenician colonies.

To suggest the mechanisms that were prominent in the Phoenician economic system in the Western Mediterranean, it is essential to understand the dynamics between the southern colonies and the northeastern indigenous communities. It seems that the Phoenicians favoured long-distance and regular commerce, and we can identify this fluid and intense presence thanks to the recovery of the first wheel-thrown pottery in indigenous contexts from the 8th century BC to ca. 575 BC. However, we lack explicit knowledge of how this system operated, and there are still many questions to be answered about the early presence of Phoenician traders in this part of the Iberian Peninsula, especially whether they established themselves in the area in permanent settlements. Additionally, we must not forget the possible role played by the southeastern indigenous potters after the arrival of Phoenician pottery since, in some cases, wheel-thrown pottery was already being made in indigenous settlements by the end of the 8th century BC [21]. The existence of such indigenous wheel-thrown pottery brings an added complexity that is only now beginning to be explored.

In 2002, the Universitat de Barcelona launched an analytical programme on Phoenician pottery recovered from different sites in Catalonia to shed light on its provenance [22]. Through this work, Sant Jaume stood out as a critical settlement in understanding the variety of Phoenician products traded during the Early Iron Age, thanks to its extraordinary state of preservation and rich assemblage, which may provide some indications about the broader dynamics at work. The results of the Central Mediterranean Phoenician pottery imports have been discussed elsewhere [23], and they suggest that the network for distributing Phoenician goods was more complex than previously thought.

This paper analyses the Western Mediterranean Phoenician imports found at this site. One of the main objectives is to determine their provenance and examine whether they were manufactured in different areas or have a much more restricted source. Typological information is also considered in studying correlations between archaeometric and archaeological data.

2. Materials and Methods

Sant Jaume (Alcanar, Montsià, Catalonia, Spain) (N 40° 35′ 4.0596; E 0° 28′ 34.1256) is an Early Iron Age settlement located on the top of a small hill (224 m AMSL) at the southern edge of the Montsià Mountains, 5 km from the mouth of the River Sénia, 20 km from the mouth of the River Ebro, and only 2 km from the coastline. It is a small site (around 700 m^2) with a remarkable defensive system [24] and a pseudo-circular plan with a single phase of occupation (6th–8th century BC). Our main hypothesis is that Sant Jaume was a fortified residence, perhaps the home and the headquarters of local political power in the framework of a chiefdom, from which it was possible to control neighbouring settlements (Moleta del Remei, la Ferradura, la Cogula, and el Castell d'Ulldecona). This chiefdom (Figure 1c) has been named the Sant Jaume Complex [25–29]. However, the work carried out in recent years at the site suggests the possibility that it could be a Phoenician factory, though further research is needed to support this hypothesis.

None of the excavated remains on the site (Figure 2) can be considered domestic units. Instead, the two-storey buildings consisted of a lower level related to stabling, the reception and processing of agricultural and livestock products and other activities, while the upper floors were used as warehouses, storing large amounts of manufactured products, raw materials, and different types of objects, including a plethora of pottery. The ceramic assemblage at Sant Jaume can be divided into two main categories: hand-made pottery, similar to that of the Late Bronze Age [30], and wheel-thrown pottery, related to that of

Phoenician colonies in the Western and Central Mediterranean Sea [23]. The wheel-thrown assemblage is composed of: T.10.1.2.1 type amphorae [31] (Figure 3a2), a new amphora type labelled as T.2.1.1.2 or similar (Figure 3a1), *pithoi* and *pithoid* vessels (Figure 3b), narrow-necked cylindrical jars of the Cruz del Negro type (Figure 3c), and, in lesser quantities, tripod mortars/vessels (Figure 3d). Besides these common types that also appear in other Iron Age settlements identified in this area, Sant Jaume also has fine tableware: carinated bowls (Figure 3e,f), plates (Figure 3g,h), red slipped jugs (Figure 3i), dipper jugs (Figure 3j), and oil bottles (this last type, only recently recovered in the excavations, is still under study and is not yet represented in the general typological table of Phoenician pieces from the site in Figure 3).

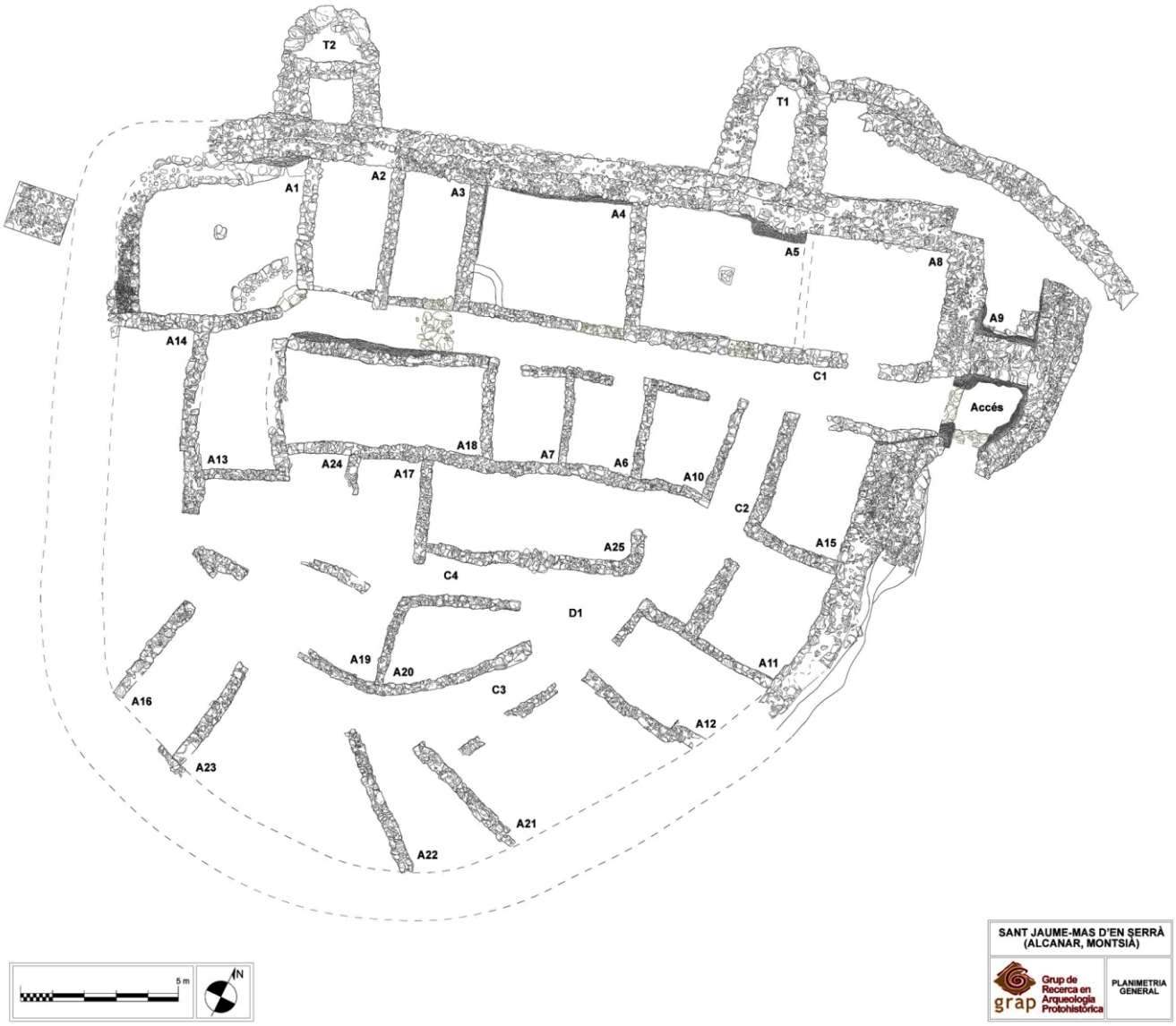

Figure 2. General plan of Sant Jaume.

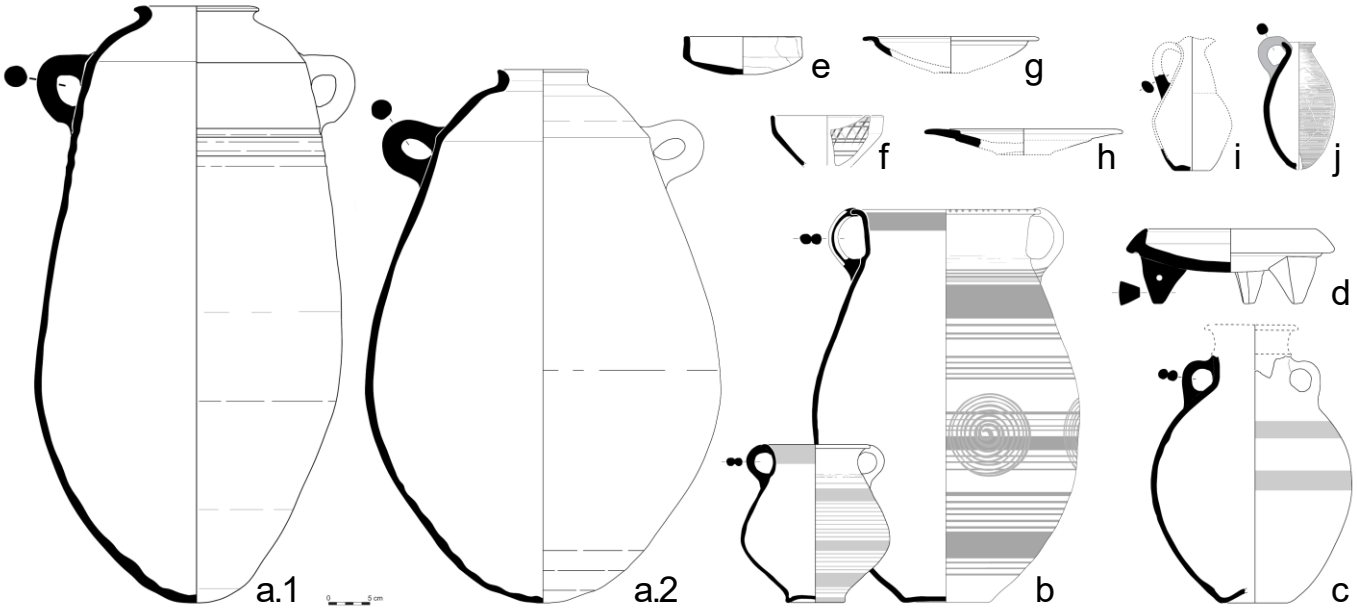

Figure 3. Wheel-thrown pottery types found at Sant Jaume. (**a1**): T.2.1.1.2 or similar amphorae. (**a2**): T.10.1.2.1 amphorae. (**b**): *pithoi* and *pithoid* vessels. (**c**): narrow-necked cylindrical jars or Cruz del Negro type. (**d**): tripod mortars/vessels. (**e**,**f**): carinated bowls. (**g**,**h**): plates. (**i**): red-slipped jugs. (**j**): dipper jugs.

The amphorae are the most common type in the collection. They mostly match Type T.10.1.2.1, which is the most common type of ancient Phoenician work in the Western Mediterranean colonies. Nevertheless, other amphora types, clearly different from the latter "canonical" type, are represented by several individuals with a much more prominent and everted rim and a tendency to a cylindrical body. We also find notable differences and variations in the *pithoi*, related to their shape and size. The highest morphological diversity is present in the narrow-necked cylindrical jars, or Cruz del Negro type, with almost every individual exhibiting different characteristics. Finally, the tripod mortars/vessels also display a marked lack of standardisation in their production.

For our study, 58 samples were taken, including especially amphorae (32), *pithoi* (5), tripod mortars (6), jars (10), plates (2), dipper jugs (1), and undetermined ceramics (2) (Table 1). These analyses complement those already published for Central Mediterranean Phoenician imports [23] (4 individuals) and hand-made pottery [30] (15 individuals, though one hand-made vessel, recently characterised, remains unpublished).

Table 1. List of individuals studied in the present paper. ID: identifier. SU: stratigraphic unit. CG: chemical groups (post-analysis); PF: petrographic fabric (post-analysis). *: observations made on individual DOV002 (not included in the present paper; see Miguel 2014). SEM: scanning electron microscopy. IV: initial vitrification; Vc−: continuous vitrification (less developed) Vc: continuous vitrification; Vc+: continuous vitrification (more developed); V: extensive vitrification.

ID	Ceramic Class	Excavation ID	SU/Area	CG	PF [1]	SEM
MOS001	Amphora	MOS1058	SJ01-1018-201	CG15		
MOS005	Amphora (T.2.1.1.2 or similar)	MOS1057	SJ01-1018-225b	CG10		Vc
MOS006	Amphora (T.10.1.2.1)	MOS1059	SJ01-1018-225a	CGTOS		
MOS007	Amphora (T.10.1.2.1)	MOS1060	SJ01-1018-225c	CGTOS		Vc/Vc+
MOS008	Jar (Cruz del Negro)	MOS1071	SJ98-9-1091	CG43		
MOS009	Amphora (T.10.1.2.1)	MOS1102	SJ01-1018-117a	CGTOS	Group 9	
MOS010	Amphora (T.10.1.2.1)	MOS1126	SJ01-1018-117b	CG15		

Table 1. *Cont.*

ID	Ceramic Class	Excavation ID	SU/Area	CG	PF [1]	SEM
MOS011	Amphora (T.2.1.1.2 or similar)	MOS1184	SJ98-0009-1135	CG10		
MOS012	Amphora (T.10.1.2.1)	MOS1185	SJ01-1018-182b	CGGUA		Vc
MOS013	Amphora (T.10.1.2.1)	MOS1196	SJ01-1018-117c	CG14		
MOS014	Amphora (T.10.1.2.1)	MOS1197	SJ01-1018-117c	CGTOS		
MOS015	Amphora (T.10.1.2.1)	MOS1198	SJ01-1018-117d	CG15		
MOS016	Amphora (T.2.1.1.2 or similar)	MOS1199	SJ01-1018-182a	CG10		
MOS019	*Pithos*	MOS1379	SJ00-1004-3254	CG44		
MOS020	Amphora	MOS1380	SJ00-1004-1474	CG13		
MOS021	Amphora	MOS1381	SJ00-1004-1460	CG14	Group 9	
MOS022	Amphora	MOS1382	SJ00-1004-557	CGGUA	Group 8	
MOS023	Amphora	MOS1383	SJ00-1004-(2 a 3)	CG13	Group 9	Vc
MOS024	Amphora	MOS1384	SJ00-1004-1461	CG15		
MOS025	Tripod-mortar	MOS1385	SJ00-1004-1466	CG21		
MOS027	*Pithos*	MOS1387	SJ01-1004-351	CG45	Group 4	
MOS029	Amphora	MOS1411	SJ01-1018-1736	CG10	Group 5	
MOS030	Tripod-mortar	MOS1412	SJ01-1004-353	CGTOS	Group 9	
MOS032	Amphora	MOS1414	SJ01-1004-397	CG10	Group 5	Vc
MOS033	Jar (Cruz del Negro)	MOS1415	SJ00-1003-1319	CG20		
MOS038	Plate	MOS1420	SJ00-1004-3152	CG46		
MOS039	Amphora	MOS1421	SJ00-1004-1468	CG47	Group 4	
MOS045	Jar (Cruz del Negro)	MOS1427	SJ01-1018-2325	CG48		
MOS047	Jar (Cruz del Negro)	MOS1429	SJ02-0000-34	CG49	Group 6	
MOS048	Tripod-mortar	MOS1430	SJ01-1001-39	CG21	Group 4	IV
MOS049	Tripod-mortar	MOS1431	SJ01-1018-2307	CG50		
MOS050	Jar (Cruz del Negro)	MOS1432	SJ01-1018-2303	CGEIV	(Group 3) *	
MOS051	Undetermined	MOS1433	SJ04-0000-116	CG51		
MOS052	Tripod-mortar	MOS1434	SJ02-1020-1020-1	CG52		
MOS053	*Pithos*	MOS1435	SJ05-2008-25	CG53		
MOS054	Jar (Cruz del Negro)	MOS1436	SJ05-1113-80	CG19		V
MOS061	Amphora	MOS1524	SJ02-1004c-44	CG14	Group 9	Vc+
MOS062	Amphora	MOS1525	SJ02-0000-4	CGTOS		Vc-
MOS063	Amphora	MOS1526	SJ02-1060-35	CG17	Group 6	
MOS064	Amphora	MOS1527	SJ02-1060-37	CGTOS	Group 9	
MOS065	Amphora	MOS1528	SJ06-0000-17	CG14	Group 9	
MOS066	Jar (Cruz del Negro)	MOS1529	SJ00-1003-(1321b, 1322b)	CG54	Group 4	
MOS067	Amphora	MOS1530	SJ00-1004-1469	CGVEL-MAG	Group 9	
MOS068	Jar (Cruz del Negro)	MOS1531	SJ05-1125-1	CG17		IV
MOS069	*Pithos*	MOS1532	SJ04-0000-142	CGGUA	Group 8	Vc
MOS070	Amphora	MOS1533	SJ00-1007-24	CG55	Group 4	
MOS071	*Pithos* or Jar	MOS1534	SJ00-1004-1535	CG20		
MOS072	Jar (Cruz del Negro)	MOS1535	SJ00-1003-261	CG56	Group 4	
MOS073	Amphora	MOS1536	SJ02-1022-12	CG14		
MOS074	Amphora	MOS1537	SJ01-1039-433	CGVEL-MAG		
MOS075	Tripod-mortar	MOS1538	SJ09-3010-89	CG57	Group 1 (?)	
MOS076	Amphora	MOS1539	BSJ05-20	CGVEL-MAG		
MOS077	*Pithos*	MOS1540	BSJ05-16	CGVEL-MAG	Group 9	
MOS078	Amphora	MOS1541	BSJ05-23	CG11		
MOS079	Jar (Cruz del Negro)	MOS1542	SJ05-1115-47	CG19	Group 4	
MOS080	Amphora (T.10.1.2.1)	MOS1543	SJ01-1018-225c	CGTOS		
MOS081	Plate	MOS1638	SJ17-2014C-18	CG67		
MOS083	Dipper jug	MOS1643	SJ18-4014D-2	CG15		

[1] Petrographic fabric in relation to chemical groups. Group 1: Rounded Quartz and Calcite: CG57 (?); Group 3: Alotriomorph Quartz and Mica Matrix: CGEIV; Group 4: Sandstone and Serpentinite: CG19, CG21; Group 5: Metamorphic and Igneous Rocks Inclusions: CG10; Group 6: Textural Concentration Features/Grog Tempered: CG17; Group 8: Serpentinite and Well-Rounded Quartz: CGGUA; Group 9: Metamorphic Rocks: CGTOS, CGVEL-MAG, CG13, CG14.

All individuals have been characterised chemically through wavelength dispersive X-ray fluorescence (WD-XRF) and mineralogically through powder X-ray diffraction (PXRD). For analysis by WD-XRF, samples of about 15 g were taken from each individual. The superficial layers were mechanically removed, and the samples were milled in a tungsten carbide cell mill, the Spex Mixermodel 8000. The chemical composition was determined from powder dried in an oven for 12 h at 105 °C. Two 30 mm glass bead replicates were made by mixing 0.3 g of the dried sample with 5.7 g of lithium tetraborate ($Li_2B_4O_7$) flux (1/20 dilution) and 5 mg of lithium iodide (LiI) as a release agent to determine the major and minor elements. This mixture was homogenised, placed in a 95% Pt, 5% Au crucible, and melted in a fully automatic bead preparation system, PANalytical Perl'X-3, at 1125 °C. Pressed powder pellets were made using 6 g of specimen mixed with 2 mL of a binding agent solution of n-butyl methacrylate synthetic resin (Elvacite® 2044) in acetone at 20% by mass to determine trace elements. This mixture was manually homogenised in an agate mortar to dryness and placed on a base of boric acid (H_3BO_3) in an aluminium vessel of 40 mm diameter subjected to a pressure of 200 kN for a period of 60 s using a Herzog press. Due to the long duration of the research project, two different XRF instruments were used to determine the concentrations. First, in the case of individuals MOS001–MOS054, a Phillips PW2400 spectrometer with an Rh excitation source was used. Then, individuals MOS061–MOS083 were analysed using an Axios^{mAX}-Advanced PANalytical spectrometer with an Rh excitation source. Both spectrometers were calibrated by a suite of 56 international Geological Standards. Interferences were considered, and matrix effects were corrected. For individuals MOS061 to MOS083, these corrections were made using the PANanalytical Pro-Trace software for trace elements. The elements determined were: Na_2O, MgO, Al_2O_3, SiO_2, P_2O_5, K_2O, CaO, TiO_2, V, Cr, MnO, Fe_2O_3 (as total Fe), Co, Ni, Cu, Zn, Ga, Rb, Sr, Y, Zr, Nb, Mo, Sn, Ba, Ce, W, Pb, and Th. For individuals MOS001 to MOS054, Na_2O was determined from the pressed powder pellet, while for individuals MOS061 to MOS083, it was determined from the glass bead replicates. Finally, for individuals MOS061 to MOS083, the trace elements Sc, La, Sm, and Yb were also determined using only PANalytical synthetic standards, and their concentrations must be considered semiquantitative. Major and minor elements are expressed as concentrations of oxides in mass fraction percentage (w%). Trace elements are expressed as elements in w mg/kg. Loss on ignition (LOI) (expressed as w%) was determined by firing 0.3 g of the dried specimen at 950 °C for 3 h. Calcinations were carried out in a Heraeus muffle model M-110 using a heating rate of 3.4 °C/min and free cooling. For the statistical data treatment, the concentrations of Mo and Sn were discarded due to analytical imprecision, as were those of Co and W because of possible contamination from the tungsten carbide cell of the mill used. P_2O_5 concentrations were not used in the data treatment as some values were considered erratic, and some individuals were pushed out of their group. Such values can be due to contamination during burial, for example, from organic matter [32] (and references therein). However, the general influence of this element was low, and the main structure defined in the data set was preserved after it was discarded. Sc, La, Sm, and Yb were discarded for the general data treatment and only used for comparison with other projects.

The mineralogical characterisation of all individuals was performed using PXRD. The previously prepared powder specimens were manually side-loaded and pressed with frosted glass in a cylindrical sample holder of 27 mm diameter and 2.5 mm high (PW 1811/27). Measurements for individuals MOS001-MOS054 were made using a Bragg-Brentano geometry diffractometer, Siemens D-500, working with the Ni-filtered Cu-Kα radiation (λ = 1.5406 Å) at a working power of 1.2 kW (45 kV and 30 mA), from (4 to 70)°2θ, at 1°2θ/min (step size = 0.05°2θ; time = 3 s). Measurements for individuals MOS061-MOS083 were made using a Bragg-Brentano geometry diffractometer PANalytical X'Pert PRO MPD Alpha-1 (radius = 240 mm) equipped with an X'Celerator detector (active length = 2.122°), using the Ni-filtered Cu-Kα radiation (λ = 1.5406 Å) at a working power of 45 kV and 40 mA, from (5 to 80)°2θ, with a 0.026° step size and an acquisition time of 50 s, spinning the sample at 1 Hz. The crystalline phases in each analysed specimen

were evaluated using the PANalytical X Pert HighScore Plus software package, which includes the Powder Diffraction FileTM (PDF®) of the International Centre for Diffraction Data (ICDD).

Twenty-three individuals (MOS009, 021, 022, 023, 027, 029, 030, 032, 039, 047, 048, 061, 063, 064, 065, 066, 067, 069, 070, 072, 075, 077, and 079) were also analysed in terms of thin section petrography (PE) at the University of Sheffield. Following Whitbread's system, petrographic groups were defined and described [33,34] (Supplementary Material 1: detailed petrographic descriptions).

Finally, a subsample of eleven individuals was studied by scanning electron microscopy with energy-dispersive X-ray spectroscopy (SEM-EDX) (MOS-005, 007, 012, 023, 032, 048, 054, 061, 062, 068 and 069) according to the classification by WD-XRF and PXRD analysis of meaningful compositional groups, by petrographic criteria, and according to specimen availability [35]. SEM-EDX observations were performed on a fresh cross-section fracture passing through the oro-aboral axis of the body wall to observe the microstructure, estimate the degree of sintering and the vitrification state of the matrix, and enable microanalysis of features of interest. Bulk specimens were fixed on metal specimen stubs using silicone adhesive, and the non-conductive ceramic specimens were made conductive. Colloidal silver paint was applied on the ceramic bulk specimen's excess silicone adhesive and lateral sides. Subsequently, the specimen surface was coated with a thin carbon film (~10 nm) by vacuum evaporation. The observations were made using JEOL JSM-6510 and Quanta 200 microscopes coupled with an energy-dispersive X-ray spectroscopy system (EDX). The observations were performed using an acceleration voltage of 20 kV and a working distance of 15 mm.

3. Results

The results of elemental concentrations determined by WD-XRF (Table 2) correspond with a particular case of the projective $d + 1$-dimensional space where the projective points are projected into the simplex $\mathbb{S}^d$. Points are represented by homogeneous coordinates that have a constant sum k ($k \in \mathbb{R}+$),

$$\mathrm{C}(\mathbf{w}) = \mathbf{x} = [x_1, \ldots, x_d, x_{d+1}] \mid x_i \geq 0 \; (i = 1, \ldots, d, d+1), x_1 + \cdots + x_d + x_{d+1} = k,$$

(in this current case, $k = 100$). The projective points' vector space is the positive orthant. Hence, for the statistical data treatment, the raw concentrations have been alr (additive log-ratio) transformed according to

$$\mathbf{x} \in \mathbb{S}^d \rightarrow \mathbf{y} = \ln\left(\frac{\mathbf{x}_d}{x_{d+1}}\right) \in \mathbb{R}^d \tag{1}$$

being $\mathbb{S}^d$ the d-dimensional simplex, and $\mathbf{x}_d = [x_1,\ldots,x_d]$. They have also been clr (centred log-ratio) transformed following the equation

$$\mathbf{x} \in \mathbb{S}^d \rightarrow \mathbf{z} = \ln\left(\frac{\mathbf{x}}{\mathrm{g}(\mathbf{x})}\right) \in \mathbb{H} \subset \mathbb{R}^{d+1}, \tag{2}$$

being $\mathbb{S}^d$ the d-dimensional simplex, g($\mathbf{x}$) the geometric mean of all $d + 1$ components of $\mathbf{x}$ and $\mathbb{H} \subset \mathbb{R}^{d+1}$ a hyperplane vector subspace of $\mathbb{R}^{d+1}$ [32,36–39].

Table 2. Chemical concentrations by WD-XRF. Major and minor elements expressed as oxides are in *w*%. Trace elements in *w* mg/kg. LOI (loss on ignition) in *w*%. b.l.d.: below the limit of detection.

	SiO_2	TiO_2	Al_2O_3	Fe_2O_3	MnO	MgO	CaO	Na_2O	K_2O	P_2O_5	LOI	V	Cr	Co	Ni	Cu	Zn	Ga	Rb	Sr	Y	Zr	Nb	Mo	Sn	Ba	Ce	W	Pb	Th
MOS001	59.83	0.79	17.22	6.63	0.16	2.17	5.18	0.67	2.44	0.19	3.81	113	108	27	45	31	134	22	101	190	29	195	17	b.l.d.	3	349	67	108	26	18
MOS005	53.87	0.99	22.76	6.57	0.05	2.39	3.55	0.90	4.40	0.20	1.61	108	116	25	44	27	84	32	207	272	30	178	24	1	10	484	76	82	25	12
MOS006	58.96	0.81	17.09	6.64	0.10	2.40	6.40	0.85	2.75	0.24	1.91	112	119	27	47	37	116	23	125	211	31	204	20	1	4	328	75	131	25	13
MOS007	60.72	0.77	15.58	6.25	0.08	2.42	6.08	0.95	2.56	0.17	1.94	110	103	28	43	32	102	22	115	232	28	202	19	1	5	321	74	260	25	12
MOS008	59.97	0.73	17.79	4.60	0.02	1.28	3.78	0.37	3.84	0.18	5.72	101	92	37	30	31	75	21	146	200	29	223	18	1	9	395	76	89	30	18
MOS009	57.48	0.84	15.59	6.90	0.11	2.43	7.36	0.73	2.61	0.22	3.95	112	101	31	45	30	110	22	117	216	34	195	20	2	8	310	69	142	23	13
MOS010	55.06	0.76	12.96	5.95	0.10	2.57	10.34	0.66	2.15	0.17	7.63	93	92	25	39	32	98	19	96	267	31	193	18	1	5	299	54	90	21	9
MOS011	53.44	1.04	22.31	6.45	0.06	2.55	4.73	1.13	4.31	0.19	1.54	107	104	28	41	24	81	30	189	272	28	171	23	1	13	423	60	148	24	11
MOS012	59.55	0.75	14.21	5.80	0.13	3.05	9.76	1.09	1.82	0.17	1.05	95	188	34	108	30	96	21	88	222	29	241	20	2	6	431	65	212	16	13
MOS013	53.74	0.85	20.69	6.89	0.13	2.51	6.98	1.07	2.30	0.21	2.78	110	145	29	46	35	270	31	105	205	33	218	19	1	3	267	70	255	30	15
MOS014	60.47	0.78	15.21	6.00	0.10	2.29	6.37	0.83	2.56	0.19	3.48	111	151	28	46	29	106	22	119	211	29	209	19	1	2	314	63	163	24	13
MOS015	55.07	0.79	17.22	7.46	0.13	2.49	7.02	0.72	2.46	0.19	4.45	117	117	25	49	39	148	25	113	228	39	204	19	1	5	285	73	61	25	13
MOS016	53.96	1.02	22.76	6.64	0.05	2.38	3.62	0.94	4.40	0.20	1.79	112	114	25	43	27	84	31	202	266	30	174	24	1	12	434	74	109	23	12
MOS019	61.65	0.82	22.41	3.97	0.02	1.37	2.05	0.37	4.25	0.30	2.17	125	100	21	44	17	91	29	183	133	33	175	21	b.l.d.	52	531	114	60	35	20
MOS020	59.45	0.84	18.89	7.27	0.16	2.46	5.57	0.74	2.54	0.19	2.39	115	116	27	50	104	183	26	104	195	36	210	19	0	5	281	90	122	23	15
MOS021	56.68	0.84	21.12	6.96	0.12	2.50	5.83	0.86	2.28	0.17	2.35	118	125	23	46	35	252	29	101	205	32	212	19	0	3	282	84	108	21	15
MOS022	60.13	0.82	14.89	6.29	0.14	3.15	10.08	0.81	2.10	0.20	1.58	104	163	29	111	36	104	21	96	229	32	229	21	0	5	490	87	116	22	14
MOS023	59.06	0.84	18.94	7.40	0.16	2.37	5.92	0.78	2.55	0.18	2.10	115	112	29	50	95	186	26	107	203	37	212	19	1	4	304	85	149	25	13
MOS024	55.53	0.78	17.61	6.95	0.16	2.78	8.10	0.70	2.52	0.19	4.76	110	111	23	49	38	129	22	107	224	37	194	18	1	3	308	68	71	24	14
MOS025	56.15	0.73	20.66	4.87	0.03	1.39	6.05	0.66	4.10	0.14	5.26	112	87	18	43	16	99	27	167	243	28	149	18	b.l.d.	7	490	88	43	33	18
MOS027	57.88	0.69	17.58	4.68	0.02	1.47	6.40	0.50	3.88	0.17	6.72	95	76	17	31	18	67	22	156	209	26	172	17	b.l.d.	7	465	95	32	34	17
MOS029	54.66	1.08	22.61	6.64	0.06	2.67	4.90	1.07	4.25	0.17	1.56	111	102	24	44	27	80	31	194	271	27	172	23	0	10	463	90	65	27	15
MOS030	62.52	0.80	15.48	6.26	0.07	2.46	5.96	0.97	2.82	0.19	2.40	107	106	20	44	33	100	20	121	231	29	200	18	0	2	406	68	73	25	14
MOS032	55.69	1.08	22.20	6.40	0.06	2.39	4.98	0.97	4.38	0.16	1.45	104	98	23	41	25	78	30	206	247	28	171	23	1	15	502	76	71	26	15
MOS033	58.18	0.68	17.62	4.67	0.02	1.50	6.19	0.41	3.83	0.11	7.52	99	76	18	32	19	66	23	154	207	25	172	17	b.l.d.	8	458	65	30	26	17
MOS038	65.19	0.66	17.70	4.70	0.02	1.23	2.31	1.13	3.59	0.16	3.11	113	88	33	30	10	72	23	148	167	26	194	18	b.l.d.	266	396	81	201	29	16
MOS039	40.46	0.50	10.33	4.07	0.07	3.28	20.03	0.47	2.67	0.23	17.73	59	49	16	34	17	54	15	83	419	21	131	14	1	1	328	50	22	13	9
MOS045	53.75	0.54	11.22	4.56	0.03	1.47	17.79	0.14	1.09	0.16	10.07	54	35	6	21	22	57	14	59	90	18	78	11	5	2	165	12	7	14	9
MOS047	54.72	0.68	18.09	5.73	0.03	1.93	7.06	0.42	3.78	0.19	6.88	115	95	30	40	18	91	22	138	134	26	188	16	b.l.d.	9	320	80	172	29	17
MOS048	55.08	0.70	20.42	4.87	0.03	1.32	6.17	0.64	3.96	0.15	6.59	111	99	19	43	18	100	25	158	231	28	146	18	b.l.d.	11	506	103	31	32	18
MOS049	58.37	0.65	16.37	5.54	0.03	1.41	7.12	0.62	3.70	0.13	5.82	94	84	19	30	16	68	22	154	215	27	203	16	b.l.d.	10	402	84	82	31	17
MOS050	50.71	0.73	15.98	4.80	0.03	1.41	16.92	0.51	2.71	0.12	6.08	82	59	16	30	16	72	22	151	259	28	200	19	1	23	357	78	77	26	15
MOS051	57.15	0.56	18.12	4.73	0.11	1.98	6.90	2.79	4.39	0.21	2.31	84	66	17	30	16	84	20	155	278	28	254	35	0	6	269	98	122	27	22
MOS052	58.70	0.72	19.96	4.71	0.02	1.47	4.70	0.53	4.37	0.15	3.90	107	93	22	30	17	73	24	173	294	23	169	17	b.l.d.	9	430	61	64	27	16
MOS053	61.37	0.83	23.45	3.95	0.02	1.56	0.98	0.36	4.06	0.10	2.53	129	119	27	46	22	88	30	180	103	34	177	21	b.l.d.	65	451	114	150	34	20
MOS054	61.79	0.69	19.16	4.40	0.02	1.39	3.69	0.47	3.86	0.18	3.57	105	88	38	32	18	78	24	161	172	25	204	17	b.l.d.	66	346	90	327	30	15
MOS061	56.13	0.89	19.83	6.97	0.12	2.80	8.38	0.75	2.42	0.18	2.47	138	121	51	49	29	223	28	110	217	35	221	19	0	7	381	89	551	19	11
MOS062	61.09	0.77	15.30	6.03	0.09	2.79	6.29	0.69	2.89	0.19	4.89	113	95	22	45	34	103	20	115	205	29	203	17	0	6	434	80	127	30	9

Table 2. *Cont.*

	SiO_2	TiO_2	Al_2O_3	Fe_2O_3	MnO	MgO	CaO	Na_2O	K_2O	P_2O_5	LOI	V	Cr	Co	Ni	Cu	Zn	Ga	Rb	Sr	Y	Zr	Nb	Mo	Sn	Ba	Ce	W	Pb	Th
MOS063	64.76	0.84	19.94	4.94	0.02	1.13	1.13	0.25	4.12	0.10	2.92	106	83	16	35	14	86	26	173	103	32	227	20	0	13	580	84	106	36	15
MOS064	60.30	0.78	16.18	6.21	0.09	2.47	6.78	0.76	2.54	0.16	4.46	122	100	21	46	35	97	20	111	206	30	198	18	1	6	352	81	101	27	9
MOS065	56.88	0.89	21.91	7.30	0.12	2.32	5.52	0.67	2.07	0.18	3.26	131	122	24	47	30	264	29	91	183	35	220	19	0	4	324	84	165	26	11
MOS066	59.25	0.72	18.30	4.77	0.03	1.46	4.66	0.33	3.83	0.12	6.89	104	77	16	34	19	64	24	165	201	29	177	17	0	13	532	70	40	33	13
MOS067	60.64	0.81	17.42	7.51	0.19	2.55	6.57	0.78	2.50	0.18	1.63	129	114	29	51	39	124	22	113	219	37	205	18	0	13	425	77	241	28	10
MOS068	67.08	0.78	18.63	4.67	0.02	1.16	1.26	0.36	3.92	0.07	2.80	99	77	37	32	16	79	24	167	103	30	210	18	0	107	506	83	443	32	13
MOS069	57.95	0.80	14.08	6.10	0.14	2.82	10.47	0.61	1.97	0.15	6.35	119	215	24	105	33	92	18	86	200	31	224	19	1	5	501	79	106	27	9
MOS070	40.57	0.53	10.23	4.14	0.06	3.35	19.94	0.26	2.37	0.15	19.59	85	71	12	34	23	47	14	79	347	20	134	12	1	6	297	51	12	16	5
MOS071	57.83	0.69	17.55	4.63	0.02	1.49	6.18	0.35	3.72	0.12	8.50	104	74	17	33	19	58	22	152	195	26	169	16	0	11	508	69	37	51	12
MOS072	58.85	0.80	21.85	4.44	0.03	1.93	3.61	0.47	4.19	0.22	4.39	127	95	24	43	19	91	28	179	213	32	169	19	0	12	529	94	161	45	14
MOS073	56.28	0.90	19.75	6.94	0.12	2.66	8.29	0.78	2.45	0.18	1.12	139	121	31	50	28	222	28	112	212	35	224	19	0	4	409	89	339	17	11
MOS074	58.93	0.81	17.67	8.22	0.19	2.25	5.82	0.62	2.47	0.22	3.50	132	113	40	50	41	133	22	111	178	42	200	18	0	7	370	83	139	33	10
MOS075	59.35	0.97	11.45	5.00	0.05	1.53	15.08	0.74	1.19	0.16	5.25	115	111	20	28	14	76	15	43	417	21	545	20	1	4	151	58	175	34	6
MOS076	59.64	0.90	18.58	7.37	0.19	2.22	5.43	0.51	2.39	0.20	3.06	137	120	29	56	41	164	25	107	196	39	220	20	0	7	487	81	179	28	10
MOS077	60.02	0.80	17.17	6.34	0.13	2.09	5.66	0.52	2.13	0.22	5.96	119	99	40	49	38	135	21	90	161	32	207	18	0	6	439	81	168	27	10
MOS078	57.25	0.87	19.58	8.15	0.20	2.05	5.55	0.41	1.61	0.22	5.01	113	116	25	50	38	212	26	63	149	40	206	18	0	6	359	79	79	36	8
MOS079	62.73	0.74	19.25	4.50	0.02	1.42	3.73	0.38	3.84	0.18	3.88	105	78	34	35	18	73	25	171	173	29	210	17	0	71	506	86	258	36	13
MOS080	61.82	0.83	16.04	6.49	0.08	2.55	6.61	0.93	2.63	0.18	2.26	131	99	26	48	33	96	21	119	246	31	207	18	0	7	404	80	195	27	10
MOS081	52.68	0.90	14.47	5.37	0.06	2.13	13.22	0.66	3.02	0.10	9.50	106	77	24	37	32	225	16	109	207	22	184	18	1	1	322	61	25	42	14
MOS083	60.23	0.86	16.37	6.63	0.15	2.46	5.38	0.66	2.60	0.22	3.52	125	117	24	53	34	94	17	98	188	29	201	21	1	2	346	86	51	22	15

The statistical treatment of the chemical data was performed using R [40]. The first analysis carried out was to calculate the variation matrix that completely determines the covariance structure of compositional data and provides the total variation (tv) of the analysed ceramic assemblage (Figure 4) [36,41]. The overall data set exhibits a total variation of 2.28, a high value that indicates a polygenic group's existence. If the total variation quantifies how different the chemical data are, the information entropy, or Shannon index, quantifies how evenly the chemical differences are related to the retained components. Here, the chemical differences are related to many components (H_2 = 3.87 Sh; H_2 % = 84.41). As can be seen in the compositional evenness graph, the elements that introduce more variability are MnO and CaO ($tv/\tau_{.j} < 0.3$) and, to a lesser extent, Na_2O, Cu, K_2O, Rb, and Zn ($0.3 < tv/\tau_{.j} < 0.5$), but no components introduce low variability ($tv/\tau_{.j} > 0.9$). Thus, total variation and compositional evenness indicate a complex structure in the data set.

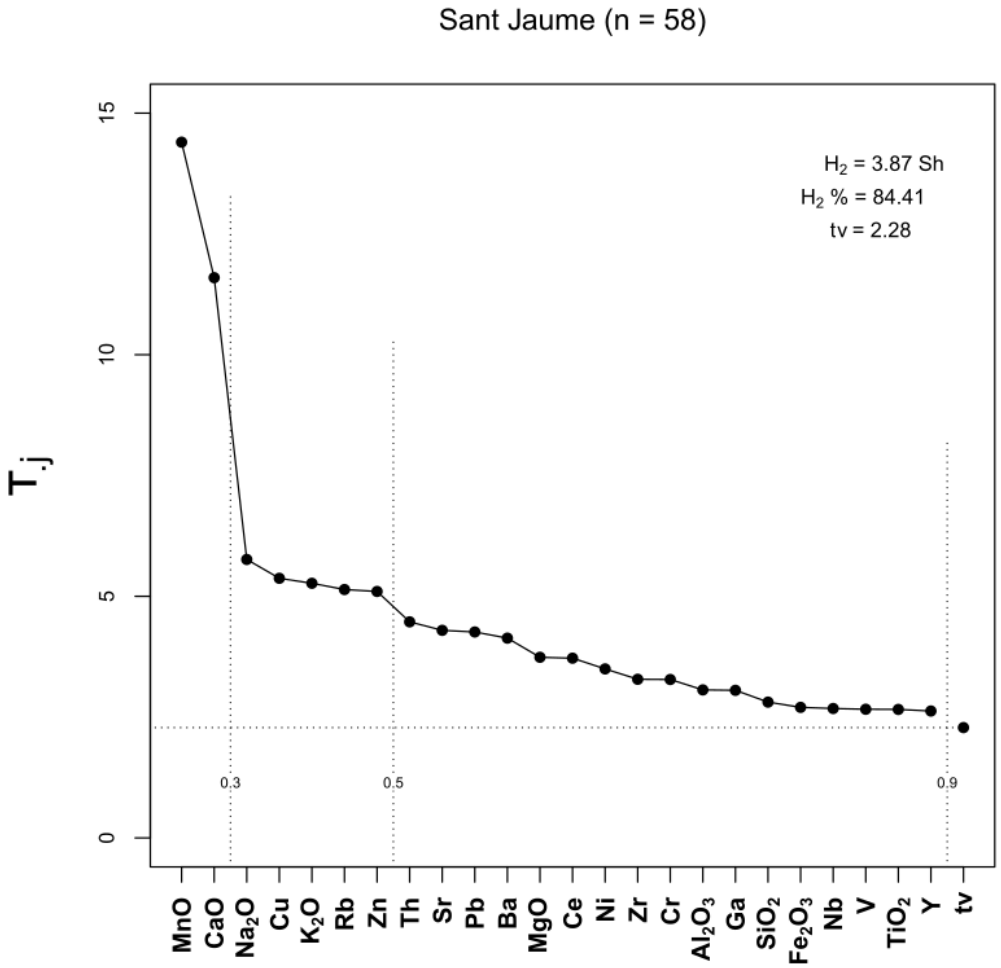

Figure 4. Compositional evenness graph of the 58 studied individuals. H_2: information entropy (in Shanons, Sh); H_2 %: percentage of the maximum possible attainable; tv: total variation. $\tau_{.j}$: trace of the variance-covariance matrix following the alr transformation using element j as the divisor. Vertical dotted lines express different $tv/\tau_{.j}$ values.

To summarise the data treatment, we present the results of the cluster analysis, using the squared Euclidean distance and the centroid agglomerative algorithm, performed on the clr transformed components: Na_2O, MgO, Al_2O_3, SiO_2, K_2O, CaO, TiO_2, V, Cr, MnO, Fe_2O_3, Ni, Cu, Zn, Ga, Rb, Sr, Y, Zr, Nb, Ba, Ce, Pb, and Th. The study of the dendrogram (Figure 5) indicates a complex structure with ten meaningful ceramic groups (or paste compositional reference units), defined as clusters of two or more individuals (plus group CGEIV, according to [22]), that account for just 33 individuals, plus 25 ungrouped

individuals because of their compositional singularities in the present data set. A higher total variation should be envisaged for such a set of compositions, but the picture suggests a complex situation of different groups (Table 3) sharing similar geological backgrounds in some cases.

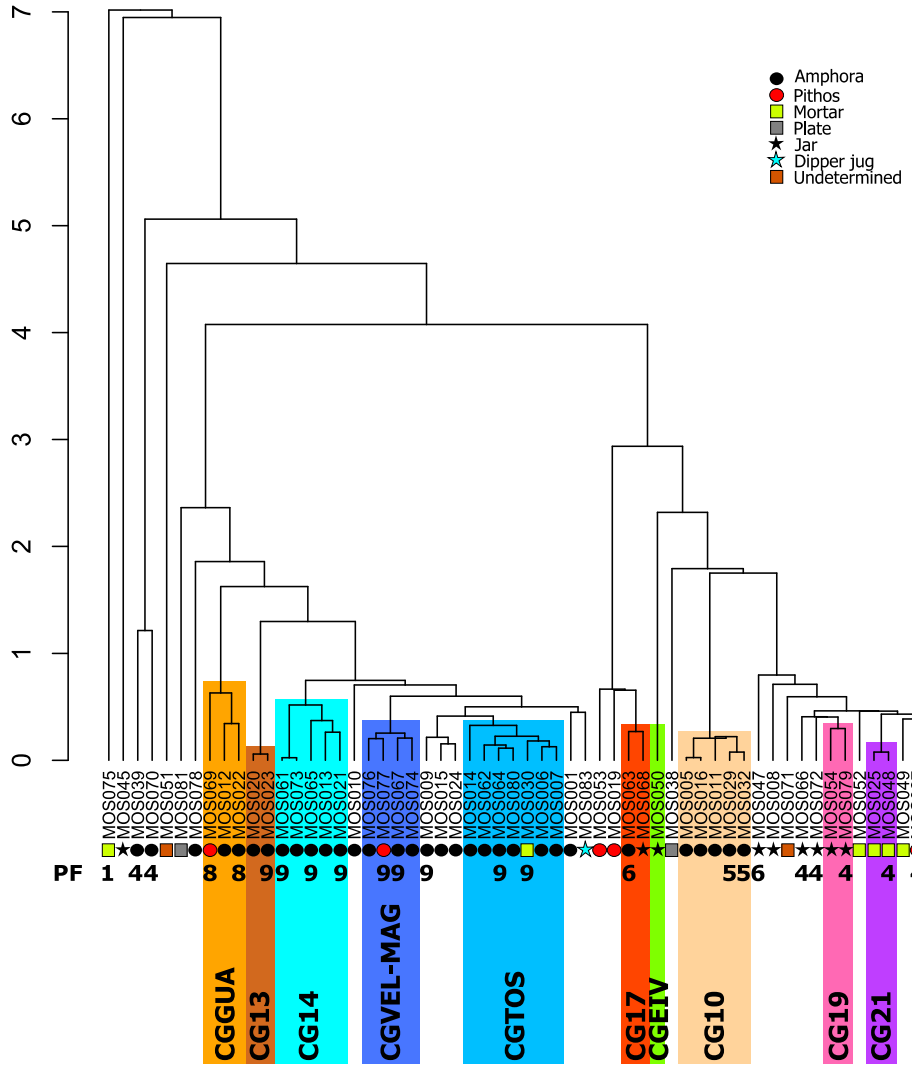

Figure 5. Dendrogram illustrating cluster analysis of the 58 individuals analysed, using the squared Euclidean distance and the centroid agglomerative algorithm, performed on the clr transformed components: Na_2O, MgO, Al_2O_3, SiO_2, K_2O, CaO, TiO_2, V, Cr, MnO, Fe_2O_3, Ni, Cu, Zn, Ga, Rb, Sr, Y, Zr, Nb, Ba, Ce, Pb, and Th. PF: petrographic fabric (post-analysis).

This structure can be understood with the biplots of the singular value decomposition on the double-centred clr transformed subcomposition Na_2O, MgO, Al_2O_3, SiO_2, K_2O, CaO, TiO_2, V, Cr, MnO, Fe_2O_3, Ni, Cu, Zn, Ga, Rb, Sr, Y, Zr, Nb, Ba, Ce, Pb, and Th (Figure 6) [42–44]. A first glance reveals that the first principal component explains 49.22% of the variance and opposes the relative values of MgO, Cu, Zn, and, especially, MnO on the right-hand side and K_2O and Rb on the left-hand one. The second principal component explains 18.13% of the variance and mainly reflects the attraction of CaO and Sr to the bottom of the biplot (Figure 6, top, left, and right). The main structure of the dendrogram (Figure 5) shows the existence of five individuals on the left, followed by two branches. The left branch corresponds to groups and individuals that exhibit high relative MnO, Zn, Cu, and MgO values, while the right branch corresponds to groups with high relative K_2O and Rb values (Tables 2 and 3), as reflected by the first principal component. Additionally,

groups and individuals are scattered from top to bottom in increasing relative values of Sr and, especially, CaO. If we draw an imaginary line from group CGGUA to group CGEIV, the individuals in the right-hand bottom corner of the biplots (Figure 6, top) correspond to those with CaO values over 9% (Tables 2 and 3), including four out of the five individuals between the two branches observed in the dendrogram (Figure 5) (MOS075, 045, 039, and 070), in the corner, and, on the imaginary line, MOS081 and MOS010, ungrouped individuals in the left-hand side branch. On the opposite top-left corner, we find group CG17 and individuals MOS053 and 019 with CaO concentrations of 2.05% or below (Tables 2 and 3), placed at the beginning of the right-hand side branch (Figure 5). Finally, the third principal component explains 8.83% of the variance and mainly reflects the increasing relative contents of Na_2O from bottom to top (Figure 6, bottom). Thus, at the bottom, individual MOS045 has a Na_2O content of 0.14%, while at the top, individual MOS051 has an extraordinarily high concentration of 2.79%. The latter is the fifth individual starting from the left on the dendrogram, just before the two branches. Besides that, the third component also shows the difference existing within the right-hand branch with group CG10 and individual MOS038 located in the upper part of the left side (Figure 6, bottom) because of their significantly higher Na_2O relative values (Tables 2 and 3).

Table 3. Mean ($\overline{X}$), standard deviation (s), and total variation (tv) of the groups of more than two individuals and the values of individual MOS050 in group CGEIV (as normalised values). Major and minor elements (expressed as oxides) in w%. Trace elements in w mg/kg.

	CGGUA (n = 3) (tv = 0.3)		**CG13 (n = 2) (tv = 0.03)**		**CG14 (n = 5) (tv = 0.26)**		**CGVEL-MAG (n = 4) (tv = 0.16)**		**CGTOS (n = 7) (tv = 0.17)**		**CG17 (n = 2) (tv = 0.14)**		**CGEIV**	**CG10 (n = 5) (tv = 0.11)**		**CG19 (n = 2) (tv = 0.16)**		**CG21 (n = 2) (tv = 0.03)**	
	$\overline{X}$	s	$\overline{X}$	s	$\overline{X}$	s	$\overline{X}$	s	$\overline{X}$	s	$\overline{X}$	s	**MOS050**	$\overline{X}$	s	$\overline{X}$	s	$\overline{X}$	s
SiO_2	61.25	0.50	60.39	0.33	57.40	0.78	61.56	1.10	63.15	0.94	67.50	1.32	53.98	56.10	0.45	64.73	0.14	59.12	0.16
TiO_2	0.82	0.03	0.86	0.00	0.90	0.02	0.85	0.05	0.82	0.02	0.83	0.05	0.78	1.08	0.03	0.74	0.03	0.76	0.01
Al_2O_3	14.89	0.19	19.28	0.02	21.20	1.04	18.23	0.63	16.44	0.67	19.75	1.05	17.01	23.27	0.50	19.97	0.10	21.83	0.06
Fe_2O_3	6.27	0.22	7.47	0.09	7.20	0.16	7.57	0.73	6.51	0.21	4.92	0.22	5.11	6.75	0.16	4.63	0.03	5.18	0.06
MnO	0.14	0.01	0.16	0.00	0.13	0.01	0.18	0.03	0.09	0.01	0.02	0.00	0.03	0.06	0.01	0.02	0.00	0.03	0.00
MgO	3.11	0.13	2.46	0.07	2.62	0.17	2.34	0.16	2.58	0.16	1.17	0.02	1.50	2.56	0.12	1.46	0.01	1.44	0.04
CaO	10.45	0.48	5.85	0.25	7.18	1.34	6.04	0.44	6.60	0.30	1.22	0.09	18.01	4.49	0.69	3.86	0.00	6.50	0.16
Na_2O	0.86	0.25	0.77	0.03	0.85	0.17	0.62	0.12	0.89	0.10	0.31	0.08	0.54	1.03	0.10	0.44	0.07	0.69	0.01
K_2O	2.03	0.13	2.59	0.01	2.36	0.15	2.44	0.14	2.78	0.14	4.12	0.17	2.88	4.49	0.11	4.00	0.05	4.28	0.06
V	110	14	117	0	130	12	133	7	119	8	105	6	87	112	4	110	1	118	1
Cr	195	31	116	3	130	12	114	8	115	21	82	4	63	110	9	86	8	99	10
Ni	112	2	51	0	49	2	53	3	47	2	34	2	32	44	2	34	2	46	1
Cu	34	3	102	6	32	4	41	1	34	2	15	1	17	27	2	19	0	18	1
Zn	101	4	188	1	253	26	143	18	107	8	84	5	77	84	4	78	5	106	2
Ga	21	2	26	1	30	2	23	2	22	1	26	2	23	32	1	26	1	28	1
Rb	93	4	107	2	107	8	108	9	122	5	174	6	161	206	8	173	6	173	5
Sr	224	12	203	6	210	13	194	23	229	15	106	1	276	274	13	180	1	252	6
Y	32	2	38	1	35	1	38	4	31	1	32	1	30	29	2	28	3	30	0
Zr	239	9	215	1	225	4	214	10	211	5	224	13	213	179	5	215	3	156	1
Nb	21	1	19	0	19	1	19	1	19	1	20	2	20	24	1	18	0	19	0
Ba	490	40	298	16	341	60	443	50	379	48	556	57	380	476	32	442	114	530	18
Ce	79	11	90	4	85	7	83	3	77	7	86	1	83	77	11	92	4	102	12
Pb	22	6	24	1	23	6	30	3	27	2	35	3	28	26	1	34	4	34	1
Th	12	3	14	1	13	2	10	1	12	2	14	1	16	13	2	14	2	19	0

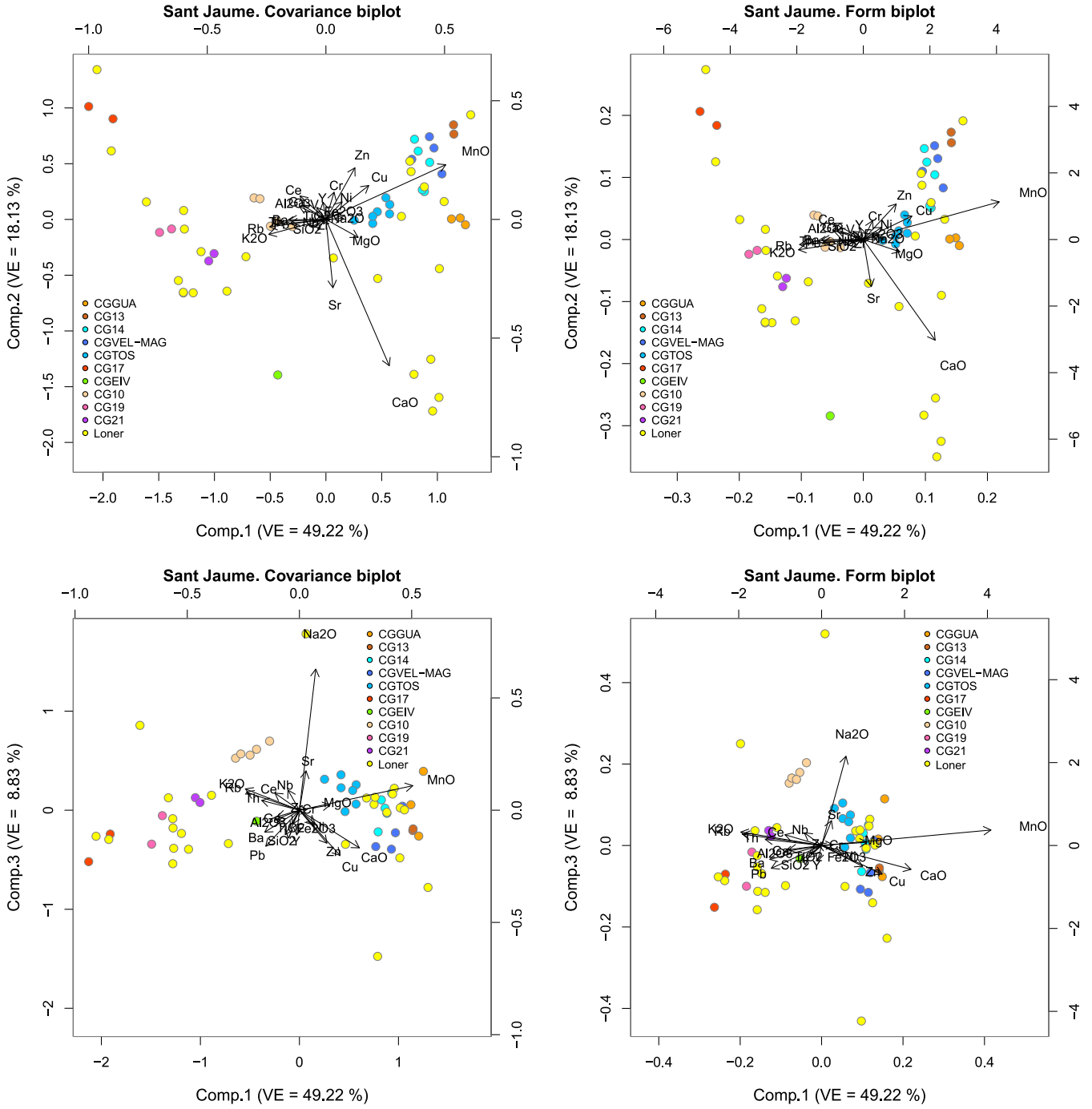

Figure 6. Biplots of the singular value decomposition on the double-centred clr transformed subcomposition Na_2O, MgO, Al_2O_3, SiO_2, K_2O, CaO, TiO_2, V, Cr, MnO, Fe_2O_3, Ni, Cu, Zn, Ga, Rb, Sr, Y, Zr, Nb, Ba, Ce, Pb, and Th. (**Top**): principal components 1 and 2. (**Bottom**): principal components 1 and 3. (**Left**): covariance biplot. (**Right**): form a biplot. VE: variance explained.

In the previous statistical treatments [22], it was possible to link some of the structures in the dendrogram resulting from the cluster analysis to production centres published by other researchers through the comparison with the existing reference groups. This comparison is semiquantitative, as only major and minor elements were considered, and there are no interlaboratory calibration studies. However, this starting point suggests possible provenances for some of our groups. Thus, it was possible to associate MOS069, 012, and 022 with Cerro del Villar (CGGUA), a Phoenician production centre in the mouth

of the Guadalhorce river [45,46]. Furthermore, we were able to relate MOS014, 062, 064, 080, 030, 006, and 007 with the site of Toscanos (CGTOS) in the Vélez river estuary, thanks to the study conducted at the Instituto di Ricerche Technologiche per la Ceramica—CNR (Faenza) on Phoenician tableware from this site [47,48]. Moreover, our data were compared with those published by the Deutsches Archäologisches Institut, performed with neutron activation analysis [49,50]. In this case, very few elements could be considered (Cr, Sc, Rb, La, Ce, Sm, Yb, and Fe_2O_3). Despite this limitation, we observed how our group CGGUA matched their group 7, which was related to Cerro del Villar, and individuals MOS076, 077, 067, and 074 appeared to be related to their group 1, connected to the area around the River Vélez, where Phoenician production centres, such as La Pancha, have been excavated. For this reason, we decided to name this group CGVEL-MAG. Finally, we compared our results with the ARQUB database, relating specimen MOS050 to the reference group of Ses Figueretes [51], a production centre on the island of Ibiza during the third century BC. This compatibility suggests that a Phoenician production centre may have existed on the island during the Early Iron Age. Phoenician T.10.1.2.1. amphorae have been analysed from the site of Via Roma (northern Ibiza), dated to the 6th century BC, whose petrographic characterisation is compatible with the island's lithology and the petrographic group defined for the Ses Figueretes workshop [52].

In the following, we present an assessment of the chemical and mineralogical data obtained through the WD-XRF, PXRD, SEM-EDX, and PE analyses for each of these groups and several particular loners (Tables 3 and 4, and Supplementary Material 1: detailed petrographic descriptions).

Table 4. Summary of the mineralogical fabrics defined by PXRD analysis for each meaningful chemical group. *n*: number of individuals. EFT: equivalent firing temperature. [PE]: Individual observed by petrography. (*): observations made on individual DOV002 (not included in the present paper; see Miguel 2014). *: Individual observed by SEM (*n* = 11). IV: initial vitrification; Vc−: continuous vitrification (less developed); Vc: continuous vitrification; Vc+: continuous vitrification (more developed); V: extensive vitrification.

PXRD Fabric	Mineralogical Assemblage	Individuals	Sintering Stage	EFT (°C)	Petrographic Fabric
Calcareous groups CGGUA (*n* = 3)					
CGGUA-I (*n* = 1)	illite-muscovite, quartz, calcite, plagioclase, gehlenite	MOS069 [PE,*]	Vc	950/1000	Group 8
CGGUA-II (*n* = 2)	quartz, plagioclase, pyroxene, hematite	MOS012 *, 022 [PE]	Vc	1000–1050	Group 8
CGTOS (*n* = 8)					
CGTOS-I (*n* = 2)	illite-muscovite, quartz, calcite, plagioclase, hematite	MOS062 *, MOS064 [PE]	Vc−	800/850	Group 9
CGTOS-II (*n* = 5)	illite-muscovite, quartz, plagioclase, pyroxene, hematite, gehlenite	MOS006, MOS007 *, MOS009 [PE], MOS014, MOS080	Vc/Vc+	900–950/1000	Group 9
CGTOS-III (*n* = 1)	quartz, calcite, plagioclase, pyroxene, hematite	MOS030 [PE]		1050	Group 9
CGVEL-MAG (*n* = 4)					
CGVEL-MAG-I (*n* = 2)	illite-muscovite, quartz, calcite, plagioclase, hematite, andalusite	MOS076, MOS077 [PE]		800/850	Group 9

Table 4. *Cont.*

PXRD Fabric	Mineralogical Assemblage	Individuals	Sintering Stage	EFT (°C)	Petrographic Fabric
CGVEL-MAG-II (*n* = 1)	illite-muscovite, quartz, calcite, plagioclase, hematite, andalusite, spessartine (?)	MOS074		800/850	
CGVEL-MAG-III (*n* = 1)	quartz, plagioclase, pyroxene, hematite, andalusite, spessartine, andradite	MOS067 [PE]		>950/1000	Group 9
CG13 (*n* = 2)					
CG13-I (*n* = 2)	illite-muscovite, quartz, plagioclase, pyroxene, hematite, andradite	MOS020, MOS023 [PE,*]	Vc	900/1000	Group 9
CG14 (*n* = 5)					
CG14-I (*n* = 3)	illite-muscovite, quartz, plagioclase, pyroxene, hematite, andalusite	MOS013, MOS021 [PE], MOS065 [PE]		850/900–950/1000	Group 9
14-II (*n* = 2)	quartz, plagioclase, pyroxene, hematite, andalusite	MOS061 [PE,*], MOS073	Vc+	1050–1080	Group 9
CGEIV (*n* = 1)					
CGEIV-I (*n* = 1)	quartz, calcite, plagioclase, pyroxene, gehlenite	MOS050		1000/1050	Group 3 (*)
CG21 (*n* = 2)					
CG21-I (*n* = 1)	illite-muscovite, quartz, calcite, plagioclase, K-feldspar	MOS025, MOS048 [PE,*]	IV	750–800	Group 4
Border-calcareous group CG10 (*n* = 5)					
CG10-I (*n* = 2)	illite-muscovite, quartz, plagioclase, hematite, K-feldspar, spinel	MOS005 *, MOS016	Vc	900/950	
CG10-II (*n* = 3)	illite-muscovite, quartz, plagioclase, hematite, K-feldspar, spinel	MOS011, MOS029 [PE], MOS032 [PE,*]	Vc	950/1000	Group 5
Low-calcareous groups CG17 (*n* = 2)					
CG17-I (*n* = 2)	illite-muscovite, quartz, plagioclase, hematite, K-feldspar	MOS063 [PE], MOS068 *	IV	750–800	Group 6
CG19 (*n* = 2)					
CG19-I (*n* = 2)	Illite-muscovite, quartz, plagioclase, hematite, spinel	MOS054 *, MOS079 [PE]	V	950/1000	Group 4

3.1. Guadalhorce Valley CGGUA

This calcareous group includes two amphorae (MOS012 and MOS022) and one *pithos* (MOS069) that can be related to the El Cerro del Villar production centre, located in the Guadalhorce Valley in Málaga [45,49]. The chemical data (Table 3) emphasise their significantly higher concentrations of Ni and Cr.

The petrographic study places the two studied individuals, MOS022 and 069, in petrographic Group 8 (Serpentinite and Well-Rounded Quartz) [22], in which the aplastic fabric component is dominated by rock fragments and the constituent minerals of metamorphic rocks (Figure 7, MOS069), where serpentinite and well-rounded quartz are the character-

istic inclusions in both the coarse and fine fractions of a calcareous matrix. Carmona [53] has previously suggested the possible exploitation of the Mio-Pliocene clays in the valley's foothills as suitable raw materials for pottery manufacture. The Guadalhorce valley presents rich areas of sand and marl with schist, quartzite, amphibolites with staurolite, disthene, sillimanite, andalusite, and serpentinite outcrops. This geological background clearly matches the petrographic characteristics of this group. From the chemical and petrographic point of view, this group bears some similarities with group FG 3 in the work of Fantuzzi and collaborators [54].

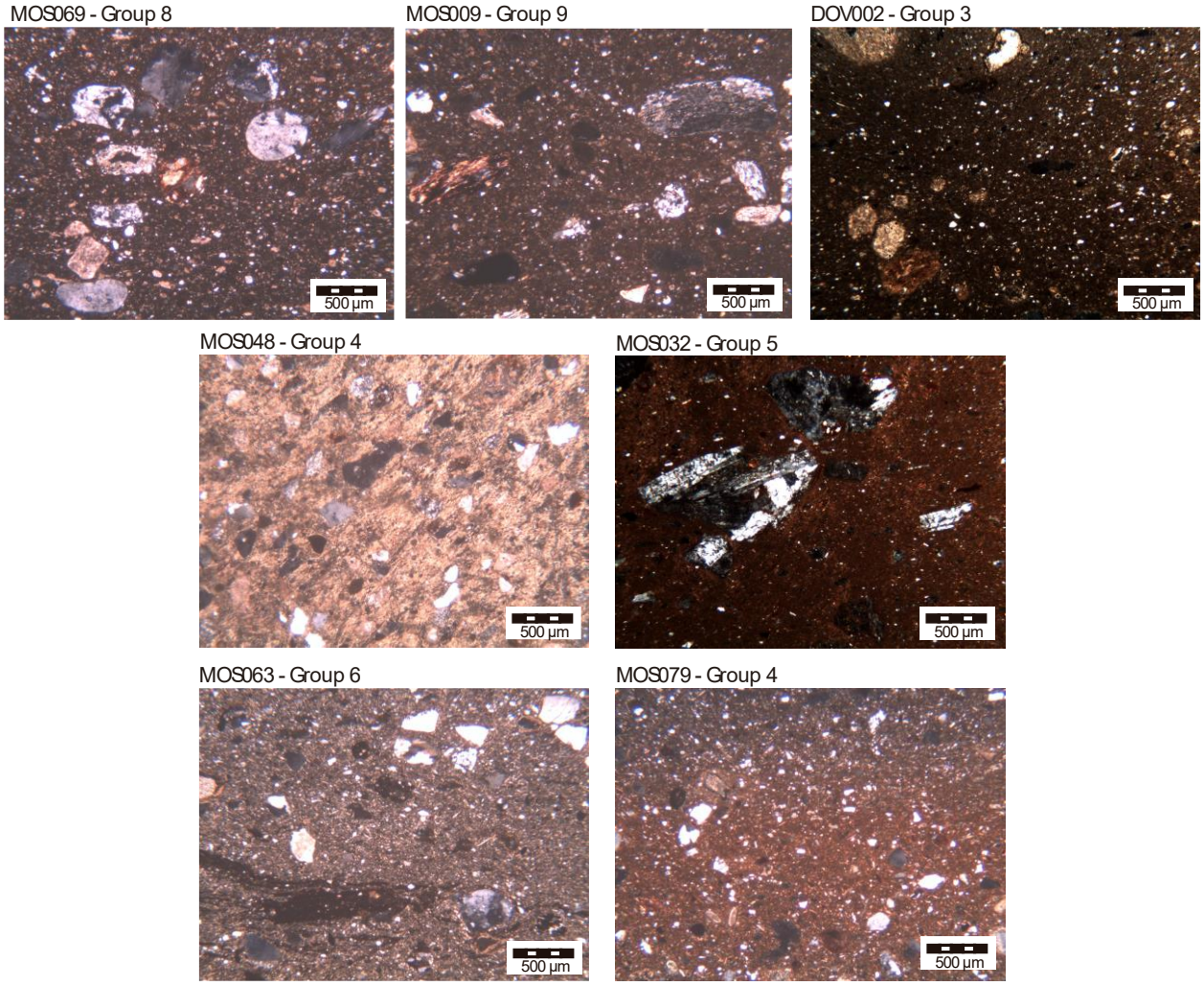

Figure 7. Photomicrographs of main petrographic fabrics (all under crossed polars, XP). Group 8: showing well-rounded quartz and micrite. MOS069 (PXRD fabric CGGUA-I) in XP (x25); Group 9: showing well-rounded inclusions of low-grade metamorphic rocks and garnets. MOS009 (PXRD fabric CGTOS-II) in XP (x25); Group 3: showing micritic calcite, small quartz, and muscovite mica. DOV002 in XP (x25) (see [22]); Group 4: showing well-sorted angular quartz, micrite, and opaques disaggregated components of sandstone. MOS048 (PXRD fabric CG21-I) in XP (x25); Group 5: showing basic igneous rock fragments. MOS032 (PXRD fabric CG10-II) in XP (x25); Group 6: showing characteristic dark textural concentration features. MOS063 (PXRD fabric CG17-I) in XP (x25). Group 4: MOS079 (PXRD fabric CG19-I) in XP (x25). Red firing member of the petrographic fabric with quartz, micrite, and white mica.

PXRD allows the identification of two different fabrics after the association of crystalline phases [35] within this calcareous group (CaO 10.45% in normalised data): CGGUA-I, represented by sample MOS069, and CGGUA-II, represented by samples MOS012 and 022

(Table 4). In the case of CGGUA-I, it is possible to estimate an equivalent firing temperature (EFT) of around (950–1000) °C on account of the absence in its diffractogram of the $d_{(002)}$ peak at 10 Å of illite-muscovite, and the presence of clear firing phases like gehlenite. Fabric CGGUA-II shows the total decomposition of illite-muscovite and gehlenite, and its EFT should be around (1000–1050) °C. This analysis confirms a differentiation observed through PE, where the micromass is optically inactive due to a possible high firing temperature.

SEM-EDX analysis of fabric CGGUA-I reveals continuous vitrification (Vc), confirming an EFT between (850–1050) °C (Figure 8, sample MOS069), the same inference that can be made for fabric CGGUA-II (Figure 8, sample MOS012).

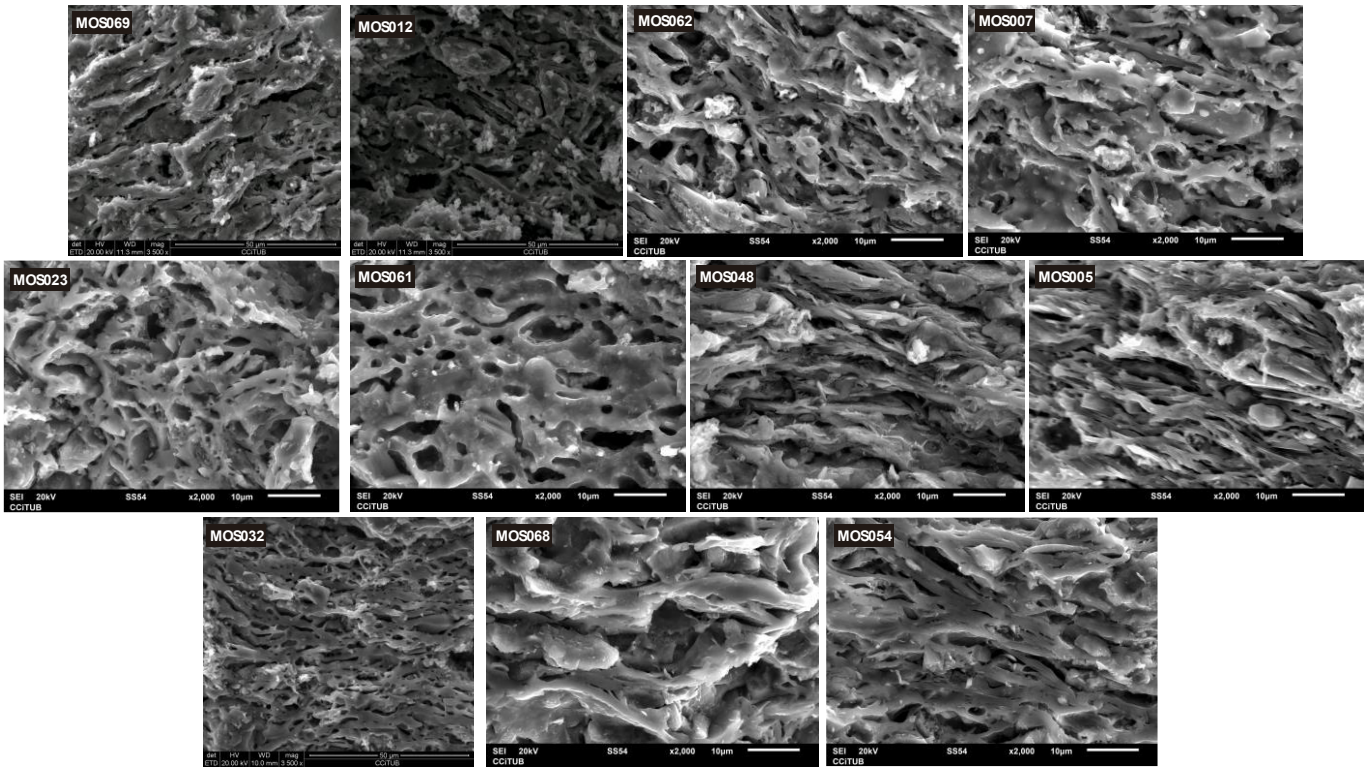

Figure 8. Photomicrographs of vitrification state estimation by SEM-EDX. MOS069 (Vc, PXRD fabric CGGUA-I). MOS012 (Vc, PXRD fabric CGGUA-II). MOS062 (Vc−, PXRD fabric CGTOS-I). MOS007 (Vc/Vc+, PXRD fabric CGTOS-II). MOS023 (Vc, PXRD fabric CG13-I). MOS061 (Vc+, PXRD fabric CG14-II). MOS048 (IV, PXRD fabric CG21-I). MOS005 (Vc, PXRD fabric CG10-I). MOS032 (Vc, PXRD fabric CG10-II). MOS068 (IV, PXRD fabric CG17-I). MOS054 (V, PXRD fabric CG19-I). IV: initial vitrification. Vc−: continuous vitrification (less developed). Vc: continuous vitrification. Vc+: continuous vitrification (more developed). V: extensive vitrification.

3.2. Toscanos CGTOS and Vélez Valley CGVEL-MAG, with Groups CG13 and CG14

Individuals MOS006, 007, 009 (at the left of the group in the dendrogram of Figure 5), 014, 062, 064, 080 (corresponding to amphorae) and MOS030 (a tripod mortar/vessel) were related in previous statistical treatments [22] to the reference group of the Phoenician site of Toscanos [47,48]. The principal chemical differences between CGGUA and CGTOS are the lower Cr and Ni concentrations in the latter, besides having the lower MnO among the ceramics in the left-hand branch of the dendrogram (Table 3). They also have different petrographic characteristics where, in contrast to the presence of serpentinite in the Guadalhorce ceramics, mica-schist is the main inclusion characterising products of the Vélez valley in what is considered Group 9 (Metamorphic Rocks). However, the distinction between different groups deriving from the area of the Vélez River is challenging, both through mineralogical and chemical means [49,50]. Archaeological remains from several

workshops in the area reflect the intensity of ceramic manufacture during the Iron Age [55]. Only in the case of CGTOS does a possible relation exist between the chemical group and the site of Toscanos, suggesting a specific, known provenance. For this reason, all samples related to the Vélez River area—several amphorae (MOS067, 074, and 076) and one *pithos* (MOS077)—but not ascribed to a specific workshop were labelled as CGVEL-MAG. Nevertheless, the significantly high CGVEL-MAG MnO concentrations separate the group from CGTOS (Table 3). The general link of the chemical composition of groups CG13 and CG14 and loners MOS010, 015, 024, 001 (amphorae), and 083 (dipper jug; see Figure 3j) with the Vélez River area should also be noted, though they vary sufficiently for their exclusion from the previous groups. For instance, group CG13 (MOS020 and 023) has high Cu and Zn concentrations (Table 3), and group CG14 (MOS013, 021, 061, 065, and 073) exhibits the highest Zn concentrations. These chemical similarities related to the Vélez-Málaga region were also detected by Behrendt and Mielke [49,50], suggesting a greater diversity in the production of this area [56]. Even if they exhibit differences, loners MOS010, 015, 024, 001, and 083 are grouped as CG15 to point to an origin in a similar geological environment, but it is important to keep in mind that this group is heterogeneous and does not seem to represent a specific production unit or location.

PE analysis shows that the main characteristic of CGTOS (including individual MOS009) and CGVEL-MAG ceramics, all classed in Group 9, is the presence of metamorphic rocks as the predominant non-plastic inclusion in a dense calcareous matrix (Figure 7, MOS009). Fragments of schist and rounded to well-rounded elongate phyllites dominate the coarse fraction, while muscovite mica, quartz, albite, and opaques indicate low-grade metamorphism. There may also be sedimentary rocks that have been changed by metamorphism, amphiboles, garnet, and hornblende that have been changed into serpentine. These petrographic characteristics are also present in groups CG13 and CG14, indicating a nearby provenance. The similarities between the geological formations of the Riff area (Morocco) and the Baetic mountain range [57] hinder a more precise determination of provenance. Previous PE studies of Phoenician ceramics found at Ceuta [58], on the African side of the Strait of Gibraltar, suggested a distinction between these two areas, contrasting the presence of ultrabasic rocks, a possible indicator of a Morocco provenance, with a low grade of metamorphics, linked to an Andalusian origin. In our case, it is not possible to suggest or reject a Moroccan provenance for groups CG13 or CG14 until we have further data from known production centres. All these groups exhibit some similarities with groups FG 4–5 [54], and, remarkably, group CG14 exhibits high Al_2O_3 and Zn concentrations.

PXRD analysis enables the identification of different fabrics (Table 4). In the case of CGTOS, the first, CGTOS-I (MOS062 and 064), has a low EFT (800–850 °C) (Figure 9, bottom left). In the case of CGTOS-II (MOS006, 007, 009, 014, and 080), the crystallisation of pyroxene and gehlenite as firing phases indicates an EFT of (900–950) °C. Finally, CGTOS-III (MOS030) has an EFT of ca. 1050 °C due to the decomposition of illite-muscovite, and gehlenite. The presence of calcite is most likely of secondary origin. From all the individuals in CGTOS, SEM-EDX analysis was performed on MOS062 (CGTOS-I), displaying less developed continuous vitrification (Vc−) with an EFT around (800–850) °C (Figure 8, MOS062), and MOS007 (CGTOS-II), exhibiting continuous vitrification, possibly advanced (Vc/Vc+), with an EFT estimated between (850/1050–1080) °C (Figure 8, MOS007).

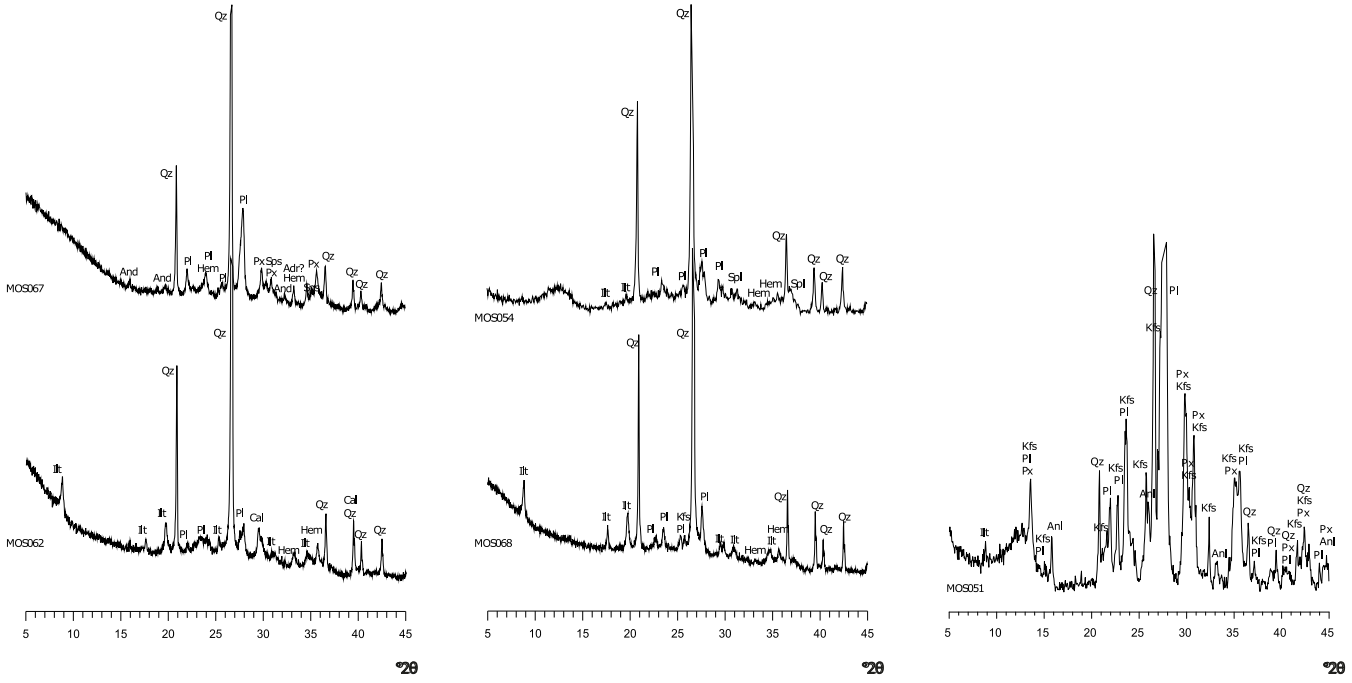

Figure 9. Examples of diffractograms of different PXRD fabrics. Bottom left: MOS062, fabric CGTOS-I. Top left: MOS067, fabric CGVEL-MAG-III. Bottom middle: MOS068, fabric CG17-I; top middle: MOS054, fabric CG19-I; right: loner CGMOS051. And: andalusite; Anl: analcime; Adr: andradite; Cal: calcite; Hem: hematite; Ilt: illite-moscovite; Kfs: K-feldspar; Pl: plagioclase; Px: pyroxene; Qz: quartz; Spl: spinel; Sps: spessartine. Abbreviations after [59] (except for Px).

PXRD of VEL-MAG reveals three different fabrics (Table 4). CGVEL-MAG-I (MOS076 and 077) has an EFT of 800–850 °C if hematite is considered a firing phase, but no clear firing phase can be observed. Andalusite, quartz, plagioclase, and illite-muscovite are also present. Fabric CGVEL-MAG-II (MOS074) is similar but exhibits spessartine, and its EFT should also be in the range of 800–850 °C. Finally, fabric CGVEL-MAG-III (MOS067) displays the absence of illite-muscovite and calcite and the presence of quartz, hematite, pyroxene, and plagioclase (Figure 9, top left). This suggests that the EFT was over 950–1000 °C. In the case of CGVEL-MAG, no SEM-EDX analysis was performed.

Group CG13 exhibits only one fabric (Table 4), CG13-I (MOS020 and 023), that, after the PXRD and SEM-EDX pieces of evidence (Figure 8, MOS023), suggests an EFT of (850/900–950/1000) °C. Finally, group CG14 has two fabrics, CG14-I (MOS013, 021, and 065) and CG14-II (MOS061 and 073), whose main difference is the presence or absence of illite-muscovite, providing two different ranges of EFT (850/900–1000) °C and over 1000 °C, respectively. The EFT estimated for CG14-II is sharpened with the information inferred from SEM-EDX (Figure 8, MOS061), which shows a Vc+ state corresponding to the range (1050–1080) °C. It is important to point out the presence of andalusite and garnets in these groups.

3.3. Ibiza: CGEIV

Based on the chemical composition, sample MOS050 is related to the Punic production centre of Ses Figueretes (Ibiza), previously studied by our group [51]. This correlation bolsters the suggestion of a Phoenician workshop in operation on the island during the Early Iron Age. Previous studies have identified such products on the Catalan coast as amphorae from Sant Martí d'Empúries. Macroscopic observations linked them to Ibiza [60], and chemical analysis confirmed this hypothesis [61]. However, pottery from Ibiza is scarce on the Catalan coast compared to that of Andalusian vessels, which are the dominant source of the whole assemblage [22].

The island of Ibiza is dominated by sedimentary and calcareous formations, mainly limestone, dolostone, and marl outcrops [51,62]. PE examination of individual DOV002 (not included in the present study; see [22]), an amphora recovered at the site of Aldovesta that is chemically related to MOS050 and therefore to group CGEIV and Group 3 (Alotriomorph Quartz and Mica Matrix) [22], suggests that this group is characterised by very rounded quartz and mica inclusions throughout its matrix. This amphora from Aldovesta (Figure 7, DOV002) contains micritic calcite with merging boundaries as the coarse fraction's dominant component, while the frequency of muscovite mica in the fine fraction stands out. Also characteristic of this fabric are clay pellets, dark orange in PPL and brown in XP (x25), with clear boundaries and high optical density, generally sub-angular and discordant with the micromass, and fine-grained non-plastic inclusions of monocrystalline quartz and calcite.

The PXRD analysis of this calcareous fabric, CGEIV-I (18.01% CaO in normalised data, Table 3), shows the presence of quartz, plagioclase, pyroxene, gehlenite, and calcite, the latter of possibly primary and secondary origin (Table 4). The absence of illite-muscovite and the presence of gehlenite suggest a high EFT in the range of (1000–1050) °C. No SEM-EDX analysis was performed on individual MOS050.

3.4. Groups without a Defined Provenance: CG21, CG10, CG17, CG19

A clear provenance could not be suggested for groups CG21, CG10, CG17, and CG19, which, together with CGEIV and twelve loners (MOS053, 019, 038, 047, 008, 071, 066, 072, 052, 049, 027, and 033), comprise the right branch of the dendrogram (Figure 5) and include most of this study's jars and tripod mortars. In contrast, the left branch of the dendrogram includes most of the amphorae. The exception is group CG10, comprised only of amphorae, whose provenance is still uncertain.

3.4.1. Group CG21

Group CG21 includes two mortars (MOS025 and 048). MOS048 is included in Group 4 (Sandstone Inclusions and Serpentinite), which reveals common sandstone fragments in the coarse and fine fractions, together with opaques and quartz (Figure 7, MOS048). This group is calcareous (6.6% and 6.37% in normalised data), and PXRD shows the presence of illite-muscovite, calcite, quartz, plagioclase, and K-feldspar phases in both individuals, indicating an EFT below (800/850) °C. Analysis of MOS048 using SEM-EDX confirmed an initial vitrification stage, confirming an EFT in the range of (750–800) °C (Figure 8, MOS048).

3.4.2. Group CG10

The five amphorae (MOS005, 011, 016, 029, and 032) of the borderline-calcareous group CG10 present some shared, characteristic morphological features, being atypical of the T-10.1.2.1 type. It can be suggested that they are not of the Phoenician type (J. Ramon personal communication), and they have been labelled as T.2.1.1.2 or similar (Table 1). The rim exhibits a much more everted shape, and they do not have the expected "baggy" body (Figure 3a1). Their provenance remains uncertain since the group's chemical composition does not match any available reference group. The PE analysis shows the presence of metamorphic and igneous rock fragments in individuals MOS029 and MOS032 conforming to Group 5 (Metamorphic and Igneous Rock), which is characterised by dominant, coarse, angular to sub-angular basic igneous rocks, some with possible trachytic texture and a distinctive yellowish to reddish mineral (Figure 7, MOS032). This phenomenon is repeated in most igneous rocks, possibly because of alteration and minerals altered to serpentine. Rounded iron oxides of red to brown colour and possible epidotes, with a hexagonal shape in MOS029, are common in the fine fraction. Elongate and well-rounded opaques with clear boundaries, angular volcanic glass with sharp boundaries, and acicular crystals are also present. There are very few to very few sub-angular to sub-rounded clinopyroxene and small monocrystalline quartz that is sub-rounded to well-rounded. Although the provenance of CG10 remains uncertain, it must be stated that intrusive igneous rocks are attested throughout the lower Guadalquivir valley along the western margins of the

Betic Cordillera [63,64], but further research is required. PXRD analysis of these border-calcareous amphorae (4.44% of CaO in normalised data, Table 3) shows two different fabrics (Table 4). CG10-I (MOS005 and 016) has illite-muscovite, K-feldspar, hematite, plagioclase, and spinel as a firing phase with an EFT of ca. (900–950) °C. For CG10-II (MOS011, 029, and 032), the $d_{(002)}$ peak at 10 Å of illite-muscovite is no longer observable, allowing us to fix an EFT between (950–1000) °C. Individuals MOS005 (CG10-I) and MOS032 (CG10-II) were studied by SEM-EDX and displayed extensive vitrification, which enabled us to confirm the PXRD EFT values (Figure 8, MOS005 and 032).

3.4.3. Group CG17

Group CG17 contains an amphora (MOS063) and a jar (MOS068), whose chemistry does not allow the ascription of provenance. PE of MOS063 shows the presence of textural concentration features or opaques as the predominant non-plastic inclusion and corresponds to Group 6 (Textural Concentration Features/Grog Tempered). These features, observed in both the coarse and fine fractions throughout the matrix, are generally dark red to opaque in PPL and brown-reddish to opaque in XP (x25), with sharp to clear boundaries and very high optical density (Figure 7, MOS063). Generally, they are very angular to sub-angular and discordant with the micromass. Sub-rounded calcite crystals and well-rounded micrite are dominant and frequent in the coarse fraction. Monocrystalline angular to well-rounded quartz is frequent in the fine fraction and white mica crystals. There is evidence of the mixing of two different clays in some parts of the thin section. PXRD analysis of these low-calcareous vessels (1.22% of CaO in normalised data, Table 3) shows a unique fabric (CG17-I), which presents a low EFT of <(800/850) °C since no firing phases are observed (Figure 9, bottom middle). Individual MOS068 was studied by SEM-EDX, exhibiting initial vitrification of the matrix (Figure 8, MOS068) that suggests an EFT estimate of (750–800) °C.

3.4.4. Group CG19

Group CG19 (two jars, MOS054 and 079) cannot be ascribed to a specific provenance. In fact, MOS079 is included in Group 4 (Sandstone Inclusions and Serpentinite), which does not contain mica-schist inclusions, suggesting a provenance other than the area of Granada and Málaga (Figure 7, MOS079). PXRD analysis of these low-calcareous ceramics (3.85% of CaO in normalised data, Table 3) produced one fabric, CG19-I, where the $d_{(002)}$ peak at 10 Å of illite-muscovite is no longer present and which contains quartz, hematite, spinel, and plagioclase phases, suggesting an EFT around (950/1000) °C (Figure 9, top middle). The SEM-EDX of MOS054 shows extensive vitrification of the matrix, confirming the EFT indicated by PXRD (Figure 8, MOS054).

3.4.5. Loners Possibly Related to These Groups

Twelve single individuals or loners (MOS053, 019, 038, 047, 008, 071, 066, 072, 052, 049, 027, and 033) (Figure 5) are possibly related to the above groups, except for group CG10, which stands clearly apart. The loners share general similarities with groups CG17, CG19, and CG21, even if several differences in their chemical composition prevent their classification in those groups. Several aspects are worthy of consideration. Individuals MOS066, 072, and 027 are classified into petrographic Group 4, as is the case with the members of chemical groups CG19 and CG21. Individuals MOS0039 and 070, on the left-hand side of the dendrogram (Figure 5), are also classified into petrographic Group 4, but their chemical composition shows more significant differences, notably much higher CaO and Sr contents. Individual MOS047 is classified into petrographic Group 6, as is individual MOS063 from chemical group CG17.

In addition to the petrographic evidence, in chemical terms, it is significant that, even if Sn was disregarded for the data treatment on account of several values below the lower limit of regression, some individuals exhibited atypically high Sn concentrations that might be diagnostic in the future for assigning provenance. Individuals MOS054 and 079 (CG19), MOS068 (CG17), and loners MOS053 and 019 have concentrations from 52 to 107 mg/kg,

while loner MOS038 goes up to 266 mg/kg (Table 2). Such concentrations might be related to areas of tin mineralisation. The Iberian Peninsula is rich in such mineralisations that have been exploited since the Bronze Age, especially in the Hesperian (or Iberian) Massif, which covers most of the western half of the Iberian Peninsula. The northwestern part of this Massif is particularly rich in such tin mineralisations forming the Iberian tin belt [65]. However, the northwest of the Iberian Peninsula, where this tin belt reaches the coast, has no evidence of western Phoenician pottery production. Within the southern part of the Hesperian Massif, two units of interest are the South-Portuguese Zone, at the southernmost side of the Massif, and the Ossa-Morena Zone, just to its north. The South-Portuguese Zone contains the Iberian Pyrite Belt (IPB), one of the largest mining districts in the world, including Sn mineralisations, for example, in the Alentejo [66]. This unit occupies the area from the province of Sevilla and south of Lisbon, almost to the Atlantic coast. In the search for tin, among other metals, the Phoenicians established several colonies on that coast, especially in the Tagus estuary, where they produced ceramics (e.g., [67,68]). Within the Ossa-Morena Zone, there is evidence of tin mining and metallurgy at Cerro de San Cristóbal (Logrosán, Cáceres, central Spain) since the Late Bronze Age [65], but also some tin ingots from the Phoenician shipwreck of del Bajo de la Campana (Cartagena, Murcia) (ca. 625–575 BC) have an origin in Los Pedroches (Córdoba) [69,70]. Finally, tin mineralisation also exists in the area of La Unión, in the coastal area of Murcia at Portman Bay [71], in the southeast of the Iberian Peninsula. However, again, there is no evidence of western Phoenician pottery production in the vicinity.

3.5. Unrelated Loners

Individuals MOS075, 045, 051, 081, and 078, at the left-hand side of the dendrogram (Figure 5), appear as loners with no relation to any defined groups. Their chemical compositions differ significantly from all other individuals and the ceramics in comparative studies. Nevertheless, two individuals must be commented on in some detail. Individual MOS051 exhibits particularly high Na_2O (2.79%) together with high K_2O (4.39%). By PXRD, the most intense peak corresponds to plagioclase, possibly albite, and it also exhibits very intense peaks of K-feldspar, pyroxene, and analcime. Quartz and illite-muscovite are also present (Figure 9, right). Unfortunately, this individual could not be studied by PE, but all the identified phases could be considered primary phases, pointing to a particular geological environment probably related to vulcanism. Individual MOS075 was classified into PE Group 1 (Rounded Quartz and Calcite Inclusions), which is related to Central Mediterranean Phoenician imports already described elsewhere [23]. However, despite its petrographic comparisons, chemical analysis reveals significant differences, though it cannot at present assign a particular provenance.

4. Discussion

Analysis of the pottery assemblage from Sant Jaume has produced compositional groups with some confidence, of which we have been able to suggest a provenance for six. The trends revealed from these ceramics, thought to be associated with Phoenician settlement and activities in the western Mediterranean, reveal some clear patterns in terms of space and time. Considering loners as potentially different groups (except those gathered together in the so-called group CG15), we have defined29 groups of wheel-made pottery, complemented by 3 groups of central Mediterranean Phoenician imports [23]. Six groups plus CG15, accounting for 28 individuals, originated in the Western Mediterranean Phoenician colonies of the southeast of the Iberian Peninsula, in the coastal areas of Málaga, Granada, and Almería, or the northern coast of Morocco (CGGUA, CGTOS, CGVEL-MAG, CG13, CG14, and CG15), and the island of Ibiza (CGEIV). The other 30 individuals account for the remaining 23 groups (groups CG21, CG10, CG17, and CG19, and 19 loners). The observed diversity in provenance provides further evidence of a complex commercial network involving a large number of pottery workshops from different geographical areas. In Figure 10, we can see that diversity is very high, with richness equal to 29, the number of

groups defined, while evenness, the distribution of individuals in each group, is considered very high (H_2 = 4.45 Sh, i.e., 91.63% of the total attainable). The high value of evenness reflects the absence of preferential consumption of goods from a single production centre, or even a small number of sources, emphasising the complex dynamic between a variety of centres, with no clear predominance of any particular Phoenician colony.

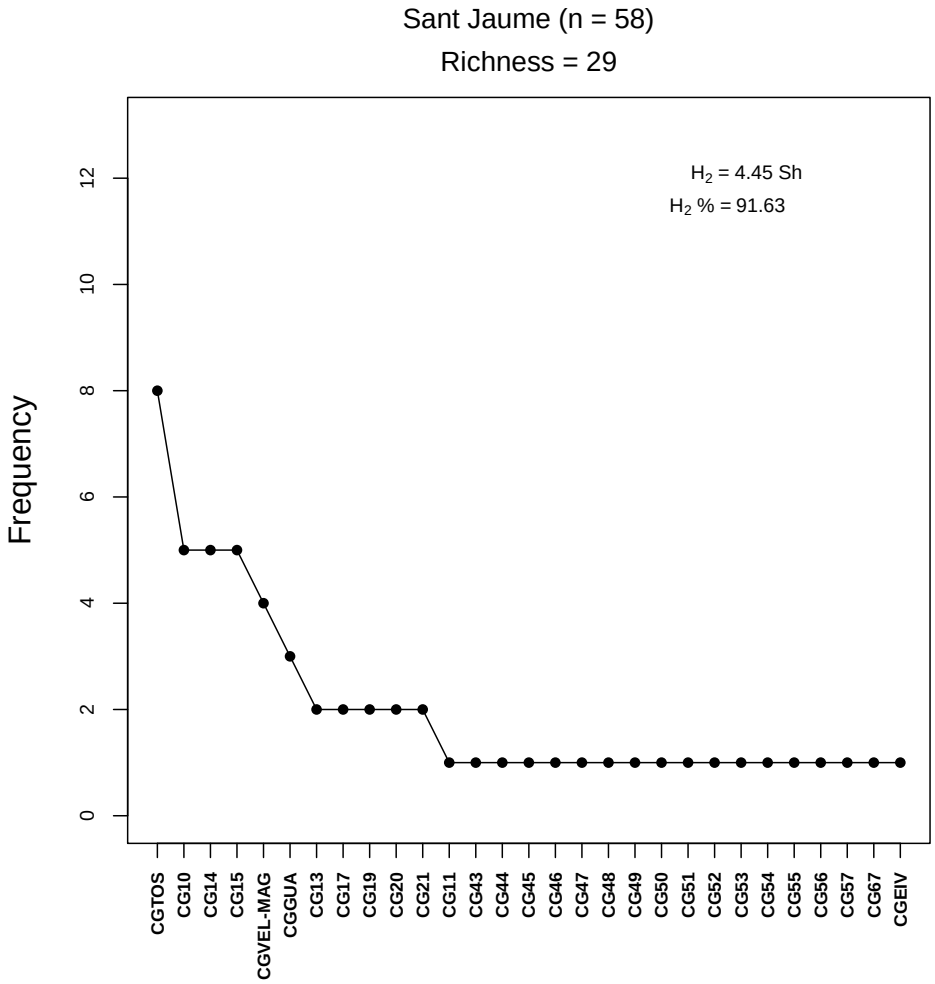

Figure 10. Rank abundance graph of the 29 defined groups based on the 58 studied individuals. H_2: information entropy (in Shanons, Sh); H_2 %: percentage of the maximum possible attainable.

There are clear indications of a large number of workshops in the south of the Iberian Peninsula that manufactured mainly amphorae; certainly, this area was the provenance most represented in transport jars at Sant Jaume, with the only significant exception being the CG10 group. It is difficult to determine more specific provenance for groups CG13 and CG14 and the outliers grouped within CG15 in that area of Andalusia (especially Málaga, Granada, and Almería provinces), where archaic Phoenician colonies were located, due to the occurence of the same geological units with similar compositional characteristics. Similarly, the geology of Morocco on its northeastern Mediterranean coast also shares similarities to that of Málaga/Granada, a problem not helped by the lack of analytical studies of pottery of this time period in Morocco, implying that we cannot rule out a north-African provenance for CG13 and CG14. Nevertheless, it has been possible to make clear distinctions between the Guadalhorce Valley (West Málaga, group CGGUA) and the Vélez Valley (East Málaga, group CGVEL-MAG) through chemical and mineralogical analyses, as well as to identify a group probably related to the Phoenician site of Toscanos (CGTOS). Although recent petrographic and chemical studies of Phoenician pottery have been carried out in Andalusia [64,72,73], we are still far from having a complete picture. Future large

analytical projects on the assemblages of Phoenician colonial sites are necessary to enhance the characterization of production units and provide crucial comparative data.

Nevertheless, some interesting differences appear if we compare the consumption patterns revealed by the analyses with those of later periods. Although we have identified the importation of pottery vessels from Ibiza (group CGEIV), these are relatively rare in this early phase on the Catalan coast. This pattern changed drastically during the Punic period [74] when Ebussitan vessels were common in Catalan-Iberian sites.

While it was not possible to suggest a provenance for most of the tripod mortars/vessels, they display great diversity. Most are not related to the area of Málaga or Granada, and two (MOS025 and 048) are members of the same group (CG21) of unknown provenance. Only MOS030 is possibly associated with the T-10.1.2.1 amphorae from Toscanos (CGTOS). It is also clear that the narrow-necked cylindrical jars, or Cruz del Negro type, do not share a provenance with that suggested for most of the amphorae. A possible provenance in Gadir and the surroundings of the Bay of Cádiz has also been ruled out, as the group does not correspond to a reference group from Camposoto (unpublished data available in our databank) or the available materials studied by other scholars. In this case, as with CG10, it has not been possible to suggest a provenance with confidence, although we can certainly say that the amphorae in group CG10 do not have their origin in the area of Málaga or Granada, an observation compatible with their variations in morphology from T-10.1.2.1 amphorae.

Previous studies have pointed out how consumption patterns among Phoenician sites in Andalusia show that the exchange between the Atlantic and Mediterranean regions was very limited [56]. In our results, even though the western Mediterranean region has a prominent role and seems to dominate the commercial network up to the northeast of the Iberian Peninsula, it is essential to keep in mind that we cannot point to a region of origin for a majority of the studied ceramics (30 out of 58). Despite this problem of sourcing the ceramics, the diversity detected would suggest it is a pattern resulting from cabotage navigation and not an exchange directed by any one Phoenician colony. Similar behaviour has been detected in the metal trade by analytical studies in the northeast of the Iberian Peninsula [75].

While we have show the emergence of important patterns of provenance for Phoenician pottery, it is equally clear that further chemical, mineralogical, and petrographic work would be beneficial beyond the Guadalhorce and Vélez Valleys and particularly on specific ceramic assemblages not only in the areas of Almería, Murcia, and Alacant but also in Morocco and on the Atlantic coast of Huelva and Portugal.

Supplementary Materials: The following supporting information can be downloaded at: https://www.mdpi.com/article/10.3390/app13063733/s1, Supplementary Material 1: Detailed petrographic descriptions.

Author Contributions: Conceptualization, E.M.G. and J.B.i.G.; methodology, E.M.G., J.B.i.G., P.M.D., and D.G.i.R.; software, J.B.i.G.; validation, E.M.G., J.B.i.G., and P.M.D.; formal analysis, E.M.G., J.B.i.G., P.M.D., and D.G.i.R.; investigation, E.M.G. and J.B.i.G.; resources, E.M.G.; data curation, E.M.G. and J.B.i.G.; writing—original draft preparation, E.M.G. and J.B.i.G.; writing—review and editing, E.M.G., J.B.i.G., P.M.D., and D.G.i.R.; visualization, E.M.G. and J.B.i.G.; supervision, E.M.G., J.B.i.G. and P.M.D.; project administration, E.M.G. and D.G.i.R.; funding acquisition, D.G.i.R. All authors have read and agreed to the published version of the manuscript.

Funding: This research was funded by (1) the Alcanar City Council, (2) the Ajuts per a projectes quadriennals de recerca en matèria d'arqueologia i paleontologia de la Generalitat de Catalunya, grant number 7495D/749000104/4431/0000 (Indígenes i fenicis. Tot calibrant l'impacte de la presència fenícia a les terres del Sénia), and (3) and Proyectos I+D+i «Generación de conocimiento» del programa estatal de generación de conocimiento y fortalecimiento científico y tecnológico del sistema de I+D+i del Ministerio de Ciencia, Innovación y Universidades, grant number PGC2018-099579-B-I00 (Complejidades crecientes. Las jefaturas politicas de la primera edad del hierro en la región del rio Senia).

Institutional Review Board Statement: Not applicable.

Informed Consent Statement: Not applicable.

Data Availability Statement: The WD-XRF and PXRD raw data presented in this study—including the semiquantitative concentrations of Sc, La, Sm, and Yb—are openly available in the CORA.RDR, Research Data Repository (https://dataverse.csuc.cat/): https://doi.org/10.34810/data632 (accessed on 14 March 2023).

Acknowledgments: WD-XRF: PXRD and SEM-EDS were performed at the *Centres Científics i Tecnològics de la Universitat de Barcelona* (CCiT). We thank the technicians of those units for their support.

Conflicts of Interest: The authors declare no conflict of interest. The funders had no role in the design of the study, in the collection, analyses, or interpretation of data, in the writing of the manuscript, or in the decision to publish the results.

References

1. Neville, A. *Mountains of Silver & Rivers of Gold. The Phoenicians in Iberia*; Oxbow Books: Oxford, UK, 2007.
2. González de Canales, F.; Serrano, L.; Llompart, J. *El Emporio Fenicio Precolonial de Huelva (ca. 900-770 a.C.)*; Biblioteca Nueva: Madrid, Spain, 2005.
3. Mederos Martín, A. Fenicios en Huelva, en el siglo X a.C, durante el reinado de Hîrām I de Tiro. *SPAL* **2006**, *15*, 167–188. [CrossRef]
4. Brandherm, D. Zur Datierung der ältersten giechischen und phönizischen Import-keramik auf der Iberischen Halbinsel. Bemerkungen zum Beginn der Eisenzeit in Südwesteuropa. *Madr. Mitt.* **2006**, *47*, 1–23.
5. Aranciba, A.; Galindo, L.; Juzgado, M.; Dumas, M.; Sánchez, V.M. Aportaciones de las últimas intervenciones a la arqueología fenicia de la Bahía de Málaga. In *Fenicios en Tartesos: Nuevas Perspectivas*; Álvarez, M., Ed.; Archaeopress: Oxford, UK, 2011; pp. 129–149.
6. Zamora, J.Á.; Gener, J.M.; Navarro, M.Á.; Pajuelo, J.M.; Torres, M. Epígrafes fenicios arcaicos en la excavación del Teatro Cómico de Cádiz (2006–2010). *Rev. Studi Fenici* **2010**, *38*, 203–236.
7. Aubet, M.E. *Tiro y las Colonias Fenicias de Occidente*; Bellaterra: Barcelona, Spain, 2009.
8. Delgado, A. Fenicios en Iberia. In *De Iberia a Hispania*; Gracia, F., Ed.; Ariel: Barcelona, Spain, 2008; pp. 347–474.
9. Martín, E.; de Dios, J.; Recio, Á.; Moreno, Á. Nuevos yacimientos fenicios en la costa de Vélez-Málaga (Málaga). *Ballix* **2006**, *3*, 7–46.
10. Schubart, H.; Niemeyer, H.G. *Trayamar: Los Hipogeos Fenicios y el Asentamiento en la Desembocadura del río Algarrobo*; Ministerio de Educación y Ciencia: Madrid, Spain, 1976.
11. Maass-Lindemann, G.; Aubet, M.E.; Schubart, H. Chorreras, un establecimiento fenicio al E. de la desembocadura del Algarrobo. *Not. Arqueol. Hispánico* **1979**, *6*, 89–138.
12. Schubart, H.; Maass-Lindemann, G. Toscanos: El asentamiento fenicio occidental de la desembocadura del río Vélez. Excavaciones de 1971. *Not. Arqueol. Hispánico* **1984**, *18*, 39–210.
13. Schubart, H.; Maass-Lindemann, G. Las excavaciones en la Necrópolis de Jardín (Vélez-Málaga, Málaga). *Cuad. Arqueol. Mediterránea* **1995**, *1*, 57–216.
14. Schubart, H. Toscanos y Alarcón, el asentamiento fenicio en la desembocadura de la ría de Vélez: Excavaciones de 1967–1984. *Cuad. Arqueol. Mediterránea* **2002**, *8*, 19–132.
15. Schubart, H.; Pingel, V. *Morro de Mezquitilla: El Asentamiento Fenicio-Púnico en la Desembocadura del Río Algarrobo*; Centro de Ediciones de la Diputación de Málaga: Málaga, Spain, 2006.
16. Maluquer, J. Los fenicios en Cataluña. Tartessos y sus problemas. In *V Symposium Internacional de Prehistoria Peninsular. Jerez de la Frontera, Septiembre 1968*; Universitat de Barcelona: Barcelona, Spain, 1969; pp. 241–250.
17. Sanmartí, E. Materiales cerámicos griegos y etruscos en las comarcas meridionales de Cataluña. *Ampurias* **1973**, *35*, 221–234.
18. Arteaga, O.; Padró, J.; Sanmartí, E. El factor fenici a les costes catalanes i del Golf de Lió, Els Pobles Pre-romans del Pirineu. In *Actes del 2º Col·loqui Internacional d'Arqueologia de Puigcerdà. Els Pobles Pre-Romans del Pirineu*; Institut d'Estudis Ceretans: Puigcerdà, Spain, 1978; pp. 129–135.
19. Arteaga, O.; Padró, J.; Sanmartí, E. La expansion fenicia por las costas de Cataluña y del Llenguadoc. In *Los Fenicios en la Península Ibérica*; Olmo, G., Aubet, M.E., Eds.; Ausa: Sabadell, Spain, 1986; Volume II, pp. 303–314.
20. Aubet, M.E. El comerç fenici i les comunitats del ferro a Catalunya. *Laietania* **1993**, *8*, 21–40.
21. Cutillas-Victoria, B.; Buxeda i Garrigós, J.; Day, P.M. Technological change and cultural resistance among southeast Iberian potters: Analytical characterisation of Early Iron Age pottery from Castellar de Librilla. *Archaeol. Anthropol. Sci.* **2021**, *13*, 174. [CrossRef]
22. Miguel Gascón, E. El Comercio Fenicio Arcaico en la Ilercavonia y la Cossetania. Proveniencia y Tecnología del Material Cerámico en un Contexto Colonial del Oeste Mediterráneo. Unpublished Ph.D. Thesis, Universidad de Zaragoza, Zaragoza, Spain, 2014.
23. Miguel Gascón, E.; Buxeda i Garrigós, J.; Day, P.M. Central Mediterranean Phoenician pottery imports in the Northeastern Iberian Peninsula. *J. Archaeol. Sci. Rep.* **2015**, *3*, 237–246. [CrossRef]
24. Garcia i Rubert, D. Els sistemes de fortificació de la porta d'accés a l'assentament de la primera edat del ferro de Sant Jaume (Alcanar, Montsià). *Rev. D'arqueologia Ponent* **2009**, *19*, 205–229.

25. Garcia i Rubert, D. Nuevas aportaciones al estudio de los patrones de asentamiento en el nordeste de la Península Ibérica durante la Primera Edad del Hierro. El caso del Complejo Sant Jaume. *Trab. Prehist.* **2011**, *68*, 331–352. [CrossRef]
26. Garcia-Rubert, D. Jefes del Sénia. Sobre la emergencia de jefaturas durante la primera Edad del Hierro en el nordeste de la península Ibérica. *Munibe Antropol.* **2015**, *66*, 223–243. [CrossRef]
27. Garcia i Rubert, D.; Moreno Martínez, I. Marcadors socials Durant el primer Ferro a Catalunya i el País Valencià. Apunts en relació amb l'assentament de Sant Jaume (Alcanar, Montsià). In *Actes del I Congrés de Joves Investigadors en Arqueologia dels Països Catalans: La Protohistòria als Països Catalans*; Miñarro, M., Valenzuela, S., Eds.; Universitat de Barcelona: Barcelona, Spain, 2008; pp. 215–225.
28. Garcia i Rubert, D.; Gracia Alonso, F.; Moreno Martínez, I. *L'assentament de la primera edat del ferro de Sant Jaume (Alcanar, Montsià). Els espais AI, A3, A4, CI, Accés i T2 del sector I.*; Edicions de la Universitat de Barcelona: Barcelona, Spain, 2016.
29. Bea, D.; Diloli, J.; Garcia i Rubert, D.; Gracia, F.; Moreno, I.; Rafel, N.; Sardà, S. Contactes i interacció entre indigenes i fenicis a les terres de l'Ebre i del Sénia durant la primera edat del ferro. In *Contactes. Indígenes i Fenicis a la Mediterrània Occidental Entre els Segles VIII I VI Ane*; Garcia i Rubert, D., Moreno Martínez, I., Gracia Alonso, F., Eds.; Ajuntament d'Alcanar/Signes disseny i Comuncació: Barcelona, Spain, 2008; pp. 135–169.
30. Barrachina, C.; Buxeda i Garrigós, J.; Garcia i Rubert, D. Caracterització arqueométricas de la ceràmica a mà del jaciment del primer ferro de Sant Jaume (Alcanar, Montsià). *Pyrenae* **2014**, *45*, 31–57. [CrossRef]
31. Ramon, J. *Las Ánforas Fenicio-Púnicas del Mediterráneo Central y Occidental*; Publicacions de la Universitat de Barcelona: Barcelona, Spain, 1995.
32. Buxeda i Garrigós, J. Alteration and contamination of archaeological ceramics: The perturbation problem. *J. Archaeol. Sci.* **1999**, *26*, 295–313. [CrossRef]
33. Whitbread, I.K. A proposal for the systematic description of thin sections towards the study of ancient technology. In *Archaeometry Proceedings of the 25th International Symposium (Held in Athens form 19 to 23 May 1986)*; Maniatis, Y., Ed.; Elsevier: Amsterdam, The Netherlands, 1989; pp. 127–138.
34. Whitbread, I.K. *Greek Transport Amphorae. A Petrological and Archaeological Study*; British School at Athens: Athens, Greece, 1995.
35. Buxeda i Garrigós, J.; Madrid i Fernández, M. Designing rigourous research: Integrating science and archaeology. In *The Oxford Handbook of Archaeological Ceramic Analysis*; Hunt, A.M.W., Ed.; Oxford University Press: Oxford, UK, 2016; pp. 19–47. [CrossRef]
36. Aitchison, J. *The Statistical Analysis of Compositional Data*; Chapman and Hall: London, UK, 1986.
37. Egozcue, J.J.; Pawlowsky-Glahn, V. Basic concepts and procedures. In *Compositional Data Analysis. Theory and Applications*; Pawlowsky-Glahn, V., Buccianti, A., Eds.; Wiley: Chichester, UK, 2011; pp. 12–28.
38. Martín-Ferández, J.A.; Buxeda i Garrigós, J.; Pawlowsky-Glahn, V. Logratio Analysis in Archaeometry: Principles and Methods. In *Mathematics and Archaeology*; Barceló, J.A., Bogdanovic, I., Eds.; CRC Press: Boca Raton, USA, 2015; pp. 178–189.
39. Buxeda i Garrigós, J. Compositional Data Analysis. In *The Encyclopedia of Archaeological Sciences*; López Varela, S.L., Ed.; John Wiley & Sons: Oxford, UK, 2018; pp. 1–5.
40. R Core Team. *R: A Language and Environment for Statistical Computing*; R Foundation for Statistical Computing: Vienna, Austria, 2021; Available online: http://www.R-project.org/ (accessed on 10 March 2023).
41. Buxeda i Garrigós, J.; Kilikoglou, V. Total variation as a measure of variability in chemical data sets. In *Patterns and Process. A Festschrift in Honor of Dr. Edward V. Sayre*; Van Zelst, L., Bishop, R.L., Henderson, J., Eds.; Smithsonian Center for Materials Research and Education: Washington, WA, USA, 2003; pp. 185–198.
42. Aitchison, J.; Greenacre, M. Biplots of compositional data. *J. R. Stat. Soc. C Appl. Stat.* **2002**, *51*, 375–392. [CrossRef]
43. Greenacre, M. *Biplots in Practice*; Fundación BBVA: Bilbao, Spain, 2010.
44. van den Boogaart, K.G.; Tolosana-Delgado, R. *Analysing Compositional Data with R.*; Springer: Berlin/Heidelberg, Germany, 2013.
45. Cardell, C. Arqueometría de las cerámicas fenicias. In *Cerro del Villar—I. El Asentamiento Fenicio en la Desembocadura del río Guadalhorce y su Interacción con el Hinterland*; Aubet, M.E., Carmona, P., Curià, E., Delgado, A., Fernández, A., Párraga, M., Eds.; Junta de Andalucía: Sevilla, Spain, 1999; Cap. CD Anexo; pp. 1–23.
46. Cardell, C.; Rodríguez Gordillo, J.; Morotti, M.; Párraga, M. Arqueometría de cerámicas fenicias de "Cerro del Villar" (Guadalhorce, Málaga): Composición y procedencia. In *Arqueometría y Arqueología*; Capel Martínez, J., Ed.; Universidad de Granada: Granada, Spain, 1999; pp. 107–120.
47. Amadori, M.L.; Fabbri, B. Produzione locale e importazioni di ceramiche fenicie da mensa (fine VIII—Fine VII secolo a. C.) a Toscanos (Spagna meridionale). In *Produzione e Circolacione Della Ceramica Fenicia e Punica nel Mediterraneo: Il Contributo Delle Analisi Archeometriche. Atti della 2ª Giornata di Archeometria Della Ceramica—Ravenna, 14 Maggio 1998 Giornatta Archeometria Della Ceramica*; Acquaro, E., Fabbri, B., Eds.; University Press Bologna: Bologna, Italy, 1998; pp. 84–85.
48. Amadori, M.L.; Del Vais, C.; Fermo, P.; Pallante, P. Archaeometric researches on the provenance of Mediterranean Archaic Phoenician and Punic pottery. *Environ. Sci. Pollut. Res.* **2017**, *24*, 13921–13949. [CrossRef]
49. Behrendt, S.; Mielke, D.P. Provenienzuntersuchungen mittels Neutronenaktivierungsanalyse an phönizischer Keramik von der Iberischen Halbinsel und aus Marokko. *Madr. Mitt.* **2011**, *52*, 139–237. [CrossRef]
50. Behrendt, S.; Mielke, D.P. Archaeometric Investigation of Phoenician Pottery from the Iberian Peninsula and Morocco using Neutron Activation Analysis. In *La vie, la Mort et la Religion dans l'univers Phénicien et Punique: Actes du VIIème Congrès International des Études Phéniciennes et Puniques*; Ferjaoui, A., Redissi, T., Eds.; Institut National du Patrimoine: Tunis, Tunisia, 2019; Volume 2, pp. 755–763.

51. Buxeda i Garrigós, J.; Cau Ontiveros, M.A. Apéndice 2. Caracterización arqueométricas de las ánforas T-8.1.3.1. del taller púnico FE-13 (Eivissa). In *FE-13: Un Taller Alfarero de Época Púnica en Ses Figueretes: Eivissa*; Ramon, J., Ed.; Museu Arqueològic d'Eivissa i Formentera: Ibiza, Spain, 1997; pp. 179–193.
52. Iliopoulos, I.; Cau, M.A.; Montana, G. Le anfore fenicio-puniche prodotte nel Mediterraneo occidentale: Caratteristiche petrografiche degli impasti siciliani e spagnoli. In *Le Classi Ceramiche. Situaione Degli Studi—Atti Della 10ª Giornata di Archeometria Della Ceramica (Roma, 5–7 Aprile 2006)*; Gualtieri, S., Fabbri, B., Bandini, G., Eds.; Edipuglia s.r.l.: Roma, Italy, 2009; pp. 157–162.
53. Carmona, P. Evolución geomorfológica del entorno del C. Villar. In *Cerro del Villar—I. El asentamiento fenicio en la desembocadura del río Guadalhorce y su interacción con el hinterland*; Aubet, M.E., Carmona, P., Curià, E., Delgado, A., Fernández, A., Párraga, M., Eds.; Junta de Andalucía: Sevilla, Spain, 1999; pp. 33–40.
54. Fantuzzi, L.; Kiriatzi, E.; Romero, A.M.S.; Müller, N.S.; Williams, C.K. Punic amphorae found at Corinth: Provenance analysis and implications for the study of long-distance salt fish trade in the Classical period. *Archaeol. Anthr. Sci.* **2020**, *12*, 179. [CrossRef]
55. Delgado, A. La producción de cerámica fenicia en el extremo occidente: Hornos de alfar, talleres e industrias domesticas en los enclaves coloniales de la Andalucía mediterránea (siglos VIII-VI a. C.). In *Yoserim: La Producción Alfarear Fenicio-Púnica en Occidente, XXV Jornadas de Arqueología Fenicio-Púnica (Eivissa, 2010)*; Costa, B., Fernández, J.H., Eds.; Museu Arqueològic d'Eivissa i Formentera: Eivissa, Spain, 2011; pp. 9–48.
56. Mielke, D.P. Between transfer and interaction: Phoenician pottery technology on the Iberian Peninsula. In *The Transmission of Technical Knowledge in the Production of Ancient Mediterranean Pottery. Proceedings of the International Conference at the Austrian Archaeological Institute at Athens, 23rd–25th November 2012*; Gauss, W., Klebinder-Gauss, G., von Rüden, C., Eds.; Österreichisches Archäologisches Institut: Wien, Austria, 2015; pp. 257–276.
57. Didon, J.; Durand-Delga, M.; Kornprobst, J. Homologies geologiques entre les deux rives du detroit de Gibraltar. *BSGF–Earth Sci. Bull.* **1973**, *S7-XV*, 77–105. [CrossRef]
58. Cau Ontiveros, M.A.; Iliopoulos, I.; Montana, G. Caracterización petrográfica de cerámica a mano y a torno del yacimiento protohistórico de la Plaza de la Catedral (Ceuta). In *El Asentamiento Protohistórico de Ceuta. Indígenas y Fenicios en la Orilla Norteafricana del Estrecho de Gibraltar*; Villada, F., Ramon, J., Suárez, J., Eds.; Archivo General de Ceuta: Ceuta, Spain, 2010; pp. 449–480.
59. Whitney, D.L.; Evans, B.W. Abbreviations for names of rock-forming minerals. *Am. Mineral.* **2010**, *95*, 185–187. [CrossRef]
60. Aquilué, X.; Castanyer, P.; Santos, M.; Tremoleda, J. Noves evidències del comerç fenici amb les comunitats indígenas de l'entorn d'Empúries. In *Contactes. Indígenes i Fenicis a la Mediterrània Occidental Entre els Segles VIII I VI Ane*; Garcia i Rubert, D., Moreno Martínez, I., Gracia Alonso, F., Eds.; Ajuntament d'Alcanar/Signes Disseny i Comuncació: Barcelona, Spain, 2008; pp. 113–134.
61. Buxeda i Garrigós, J.; Tsantini, E. Les àmfores ibèriques del derelicte de Cala Sant Vicenç i la seva contrastació amb les àmfores de la Palaià Polis d'Empúries. Evidències des de la seva catacterització arqueométricas. In *El Vaixell Grec Arcaic de Cala Sant Vicenç*; Nieto, X., Santos, M., Eds.; Museu d'Arqueologia de Catalunya, Girona: Girona, Spain, 2008; pp. 373–396.
62. IGME. *Mapa Geológico de España 1:200.000, hojas 49-65, Menorca-Ibiza-Formentera*; Instituto Geológico y Minero de España: Madrid, Spain, 1972.
63. Domínguez-Bella, S. Estudio de las materias primas en la Prehistoria del ámbito gaditano. In *Actas del I Seminario Hispano-Marroquí de Especialización en Arqueología*; Bernal, D., Raissouni, R., Ramos, J., Bouzouggar, A., Eds.; Servicio de Publicaciones de la Universidad de Cádiz: Cádiz, Spain, 2006; pp. 77–87.
64. Johnston, P.A. Pottery Production at the Phoenician Colony of El Castillo de Doña Blanca (El Puerto de Santa María, Spain) c. 750-550 BCE. Ph.D. Thesis, Harvard University, Cambridge, MA, USA, 2015.
65. Comendador Rey, B.; Meunier, E.; Figueiredo, E.; Lackinger, A.; Fonte, J.; Fernández Fernández, C.; Lima, A.; Mirão, J.; Silva, R.J.C. Northwestern Iberian Tin Mining from Bronze Age to Modern Times: An overview. In *The Tinworking Landscape of Dartmoor in an European Context—Prehistory to 20th Century*; Newman, P., Ed.; Short Run Press: Sowtonm, UK, 2017; pp. 133–153.
66. Reiser, F.K.M.; Rosa, D.R.N.; Pinto, Á.M.M.; Carvalho, J.R.S.; Matos, J.X.; Guimarães, F.M.G.; Alves, L.C.; de Oliveira, D.P.S. Mineralogy and geochemistry of tin- and germanium-bearing copper ore, Barrigão re-mobilized vein deposit, Iberian Pyrite Belt, Portugal. *Int. Geol. Rev.* **2010**, *53*, 1212–1238. [CrossRef]
67. Arruda, A.M. Phoenicians in Portugal. In *The Oxford Handbook of the Phoenician and Punic Mediterranean*; Doak, B.R., López-Ruiz, C., Eds.; Oxford University Press: Oxford, UK, 2019; pp. 603–616. [CrossRef]
68. Fernández, F.J.G.; Filipe, V.; Megías, V.M.; Del Río, J.J.M.; Alés, V.F.; Fernandes, L. Producción e importación de contenedores anfóricos en la antigua Olisipo durante la Edad del Hierro e inicios de la Romanización: Caracterización arqueométrica. *Cuad. Prehist. Y Arqueol. Univ. Autónoma Madr.* **2021**, *47*, 151–179. [CrossRef]
69. Mederos Martín, A.; Chamón Fernández, J.; García Alonso, J.I. Análisis de isótopos de plomo de lingotes de estaño del pecio fenicio del Bajo de la Campana (Murcia, España). In *Mazarrón II. Contexto, Viabilidad y Perspectivas del Barco B-2 de la Bahía de Mazarrón: En homenaje a Julio Mas García*; Iniesta Sanmartín, A., Martínez Alcalde, M., García Cano, J.M., Blánquez Pérez, J., Eds.; Universidad Autónoma de Madrid: Madrid, Spain, 2017; pp. 429–443.
70. Montes-Landa, J.; Montero-Ruiz, I.; Castanyer Masoliver, P.; Santos Retolaza, M.; Tremoleda Trilla, J.; Martinón-Torres, M. Traditions and innovations: Versatility of copper and tin bronze making recipes in Iron Age Emporion (L'Escala, Spain). *Archaeol. Anthropol. Sci.* **2020**, *12*, 124. [CrossRef]

71. López García, J.A.; Oyarzun, R. *The old Mazarrón and La Unión Pb-Zn orefields—SE Spain: A Travel into the Past and a Field and Teaching Guide. Some Insights into the History, Geology, Ore Deposits, Mining and Environmental Issues*; Ediciones GEMM–Aula2puntonet: Madrid, Spain, 2018.
72. Krueger, M.; Brandherm, D. Early Iron Age pottery in south-western Iberia: Archaeometry and chronology. In *Networks of Trade in Raw Materials and Technological Innovations in Prehistory and Protohistory: An Archaeometry Approach. Proceedings of the XVII UISSPP World Congress (1–7 September 2014, Burgos, Spain)*; Delfino, D., Piccardo, P., Baptista, J.C., Eds.; Archaeopress: Oxford, UK, 2016; pp. 95–103.
73. Krueger, M.; Moreno, V. La transición Bronce Pleno—Orientalizante en Setefilla (Lora del Río, Sevilla): Datos arqueométricos de una secuencia estratigráfica. *Estud. Arqueol. De Oeiras* **2021**, *29*, 25–32.
74. Sanmartí, J.; Asensio, D. Fenicis i púnics al territory de Catalunya: Cinc segles d'interacció colonial. *Fonaments* **2005**, *12*, 89–105.
75. Rafel, N. La cuenca minera del Baix Priorat (Tarragona): Exploration y distribución en época colonial. Recursos locales versus recursos alóctonos. *Cuad. Arqueol. Mediterránea* **2013**, *21*, 71–85.